arXiv:1411.5645v1 [hep-ph] 20 Nov 2014

Type II Seesaw Higgsology and LEP/LHC constraints

Abdesslam Arhrib,[1] Rachid Benbrik,[2] Gilbert Moultaka*,[3] and Larbi Rahili[4]

[1]*Département de Mathématiques, Faculté des Sciences et Techniques, Tanger, Morocco*

[2]*Faculté Polydisciplinaire, Université Cadi Ayyad, Sidi Bouzid, Safi-Morocco*

[3]*Laboratoire Charles Coulomb (L2C) UMR 5221*

CNRS-Univ. Montpellier 2, Montpellier, F-France

[4]*Laboratoire de Physique des Hautes Energies et Astrophysique,*

Université Cadi-Ayyad, FSSM, Marrakech, Morocco

(Dated: November 21, 2014)

* corresponding author

Abstract

In the *type II seesaw* model, if spontaneous violation of the lepton number conservation prevails over that of explicit violation, a rich Higgs sector phenomenology is expected to arise with light scalar states having mixed charged-fermiophobic/neutrinophilic properties. We study the constraints on these light CP-even (h^0) and CP-odd (A^0) states from LEP exclusion limits, combined with the so far established limits and properties of the $125 - 126$ GeV $\mathcal{H}$ boson discovered at the LHC. We show that, apart from a fine-tuned region of the parameter space, masses in the ~ 44 to 80 GeV range escape from the LEP limits if the vacuum expectation value of the Higgs triplet is $\lesssim \mathcal{O}(10^{-3})$GeV, that is comfortably in the region for 'natural' generation of Majorana neutrino masses within this model. In the lower part of the scalar mass spectrum the decay channels $\mathcal{H} \to h^0 h^0, A^0 A^0$ lead predominantly to heavy flavor plus missing energy or to totally invisible Higgs decays, mimicking dark matter signatures without a dark matter candidate. Exclusion limits at the percent level of these (semi-)invisible decay channels would be needed, together with stringent bounds on the (doubly-)charged states, to constrain significantly this scenario. We also revisit complementary constraints from $\mathcal{H} \to \gamma\gamma$ and $\mathcal{H} \to Z\gamma$ channels on the (doubly)charged scalar sector of the model, pinpointing non-sensitivity regions, and carry out a likeliness study for the theoretically allowed couplings in the scalar potential.

PACS numbers:

I. INTRODUCTION

Since the major discovery of a new bosonic particle at the LHC, [1], [2], denoted hereafter by $\mathcal{H}$, evidence has been accumulating in favor of it being Standard Model (SM) Higgs-like that culminated by the analyses of the full data sets of the LHC Run 1, both of the fit of its couplings to the SM gauge bosons and fermions [3], [4] and of the determination of its intrinsic spin and parity properties [5], [6, 7], and is being continuously confirmed through the most recent results [8, 9]. On the other hand, the so far negative direct searches for physics beyond the SM (BSM) tend to become somewhat intriguing as the emblematic TeV scale limits are crossed. Nonetheless, various degrees of model assumptions go into these exclusion limits, and the LHC Run 2 is feverishly awaited, to improve on them or, better, to discover new physics that could be revealed through more subtle kinematic configurations.

In either case, one of the most important task in the coming years, with accumulated data and increased precision at the LHC, will be to improve on our experimental understanding of the properties of the $\mathcal{H}$ boson, particularly in the not yet well tested heavy fermion sector; should they come ever closer to the SM expectation, then BSM models that predict naturally this behavior would become particularly attractive.

The Higgs sector of the *type II seesaw* model of Majorana neutrino masses [10–14] provides such a behavior, making of it an interesting phenomenological setting for an extended Higgs sector. Indeed, the interplay between the $SU(2)_L$ doublet and triplet scalar states present in this model, together with the large hierarchy between the associated vacuum expectation values accounting for the hierarchy between the neutrino masses and the electroweak scale, imply *naturally* that one of the scalar states is almost a SM Higgs, i.e. with tree-level couplings to matter and gauge bosons deviating only by $\mathcal{O}(m_\nu/M_{top})$ from the SM ones. We stress that this comes about without the need of a 'decoupling regime' entailing heavy BSM degrees of freedom, [in contradistinction with some of the other fashionable BSM models relying on supersymmetric, extra space dimensional, or compositeness scenarios.] The other predicted scalar states of the model could thus still be accessible at the LHC energies, in particular a distinctive doubly charged state, as well as a singly charged, a CP-even and a CP-odd neutral states, *even if* $\mathcal{H}$ *would become more and more compatible with the SM.* However these new states, whether charged or neutral, are typically not easy to produce and correspondingly to exclude. Their single production cross-sections are suppressed by

$\mathcal{O}(m_\nu^2/M_{top}^2)$ for the same reason as above, and one has to resort to the unsuppressed pair production with less available phase space.

The discovered $\mathcal{H}$ boson can be identified either with the lighter CP-even scalar state of the model, h^0, or with the heavier H^0.[1] In the following we will refer to these two possibilities respectively as the h^0-, H^0-*scenario*. The distinction between the h^0-*scenario* and the H^0-*scenario* is parametrically controlled by the relative magnitudes of the explicit and spontaneous lepton number violating (LNV) parameters present in the model [15]. It can thus have a bearing on the ultraviolet (UV) completion that underlies the dynamical origins of these two sources of LNV. Choosing phenomenologically the magnitude of explicit violation to be of the same order or (much) smaller than spontaneous violation, resulting respectively in the h^0-, H^0-*scenarios* with electroweak scale scalar masses, can be theoretically justified in models where the two sources of LNV are dynamically related (with, for instance, a loop induced effective LNV). In contrast, the h^0-*scenario* was initially motivated by the conventional assumption that the mass parameters in the triplet sector are of order the grand unification (GUT) scale, leading to a triplet sector (including explicit LNV) that is too heavy to be relevant at the electroweak scale. Even in such settings where the origin of the explicit lepton number violation is dynamically unrelated to that of spontaneous violation, one can obviously still motivate light triplet states by assuming an UV completion much lighter than the GUT scale. In this case the magnitude of the explicit violation can again be comparable to or smaller than that of spontaneous violation, so that both h^0-, H^0-*scenarios* can occur.

Most of the recent phenomenological studies have assumed the h^0-*scenario* [16],[17], [18], [19], [20], [21]. In the present paper we consider both scenarios but focus more on the H^0-*scenario*. In the latter, the lighter CP-even and CP-odd states, h^0, A^0, become essentially degenerate with a mass below 125GeV, while the charged and doubly-charged states $H^\pm, H^{\pm\pm}$ can lie anywhere above their present exclusion limits. It will thus be important to take into account all present direct and indirect experimental constraints in the Higgs sector in order to narrow down the viable parameter space regions of the H^0-*scenario*. In particular, stringent exclusions come from the LEP limits on direct searches for light scalar and

[1] Note that there is also the possibility that these two states be essentially degenerate, each carrying an equal fraction of the SM-like couplings, however this occurs in an extremely fine-tuned region of the parameter space.

pseudo scalar states as well as from the Z-boson width. Improving the measurement of the $\mathcal{H}$ production cross-sections and decays into W, Z gauge bosons and fermions, as expected at the LHC Run 2, will not constrain significantly the model. The $\gamma\gamma$ (and $Z\gamma$) decay channels will be in principle more sensitive to the extended scalar sector through the charged and doubly charged states loop effects. We will show, however, that these loop effects can still be blind to nearby (doubly) charged states due to a somewhat generic regime of destructive interference present in both h^0-, H^0-*scenarios*. Direct searches for (doubly) charged states become then particularly compelling. In the H^0-*scenario*, though, further constraints will come from LHC limits on invisible/undetected $\mathcal{H}$ decays into pairs of h^0 or A^0. One of the main results of this paper will be that the H^0-*scenario* is particularly difficult to exclude. Parts of its parameter space that are favored by the smallness of neutrino masses totally evade the LEP exclusion limits on light states. To narrow down the allowed parameter space would require achieving very strict limits on invisible/ undetected $\mathcal{H}$ decays combined with increased lower bounds on the (doubly)charged Higgs masses states from direct searches at the LHC, while the other decay channels of $\mathcal{H}$ will have a marginal impact as they remain essentially SM-like.

The rest of the paper is organized as follows: in Section II we recall the main ingredients of the scalar potential, the physical scalar states and their mass spectrum and couplings, distinguishing explicitly the model parameter domains corresponding to the h^0- and H^0-*scenarios*. We also describe briefly possible UV-completions of the less conventional H^0-*scenario*. Section III is devoted to a re-analysis of the $\gamma\gamma$ and $Z\gamma$ Higgs decay channels within our model. We provide a general parameterization that encompasses the two channels and the two $\mathcal{H}$-*scenarios* and discuss the charged and doubly charged scalar states loop effects. We revisit the correlation between the two decay channels and its phenomenological incidence, given the foreseen future experimental low precision on the $Z\gamma$ channel. We also demonstrate the existence of a generic screening of the charged scalar loop effects. Section IV is devoted to a study of the likeliness of the various parameter space regions of the relevant couplings as dictated by the unitarity and vacuum stability (U-BFB) constraints in the scalar potential. A detailed phenomenological study of the H^0-*scenario* with the CP-even and CP-odd scalar states lighter than $\mathcal{H}$, is carried out in section V, taking into account LEP and LHC constraints. Section VI contains the conclusions, and some technical material is given in the appendices.

II. THE MODEL

The *type II seesaw* model[2] consists of the Standard Model with an additional colorless $SU(2)_L$ triplet scalar field Δ with hypercharge $Y_\Delta = 2$. Denoting by H the standard scalar field $SU(2)_L$ doublet and taking the 2×2 traceless matrix representation for the triplet Δ we write the two multiplets in terms of complex valued scalar components as,

$$H = \begin{pmatrix} \phi^+ \\ \phi^0 \end{pmatrix}, \qquad \Delta = \begin{pmatrix} \delta^+/\sqrt{2} & \delta^{++} \\ \delta^0 & -\delta^+/\sqrt{2} \end{pmatrix} \tag{2.1}$$

with the conventional electric charge assignment for the doublet and following $Q = I_3 + \frac{Y}{2}$ with $I_3 = -1, 0, 1$ for the triplet. The Lagrangian of the model reads

$$\mathcal{L} \;=\; (D_\mu H)^\dagger (D^\mu H) + Tr\{(D_\mu \Delta)^\dagger (D^\mu \Delta)\} - V(H,\Delta) + \mathcal{L}_{\rm Yukawa} + \mathcal{L}_{\rm Gauge} \tag{2.2}$$

where

$$D_\mu H \;\equiv\; \partial_\mu H + igT^a W_\mu^a H + i\frac{g'}{2} B_\mu H \tag{2.3}$$

$$D_\mu \Delta \;\equiv\; \partial_\mu \Delta + ig[T^a W_\mu^a, \Delta] + ig'\frac{Y_\Delta}{2} B_\mu \Delta \tag{2.4}$$

$(W_\mu^a,\ g)$, and $(B_\mu,\ g')$ denoting respectively the $SU(2)_L$ and $U(1)_Y$ gauge fields and couplings and T^a the $SU(2)$ generators in the fundamental representation. The most general renormalizable potential consistent with all the symmetries of the model is given by

$$\begin{aligned} V(H,\Delta) \;=\; & -m_H^2 H^\dagger H + \frac{\lambda}{4}(H^\dagger H)^2 + M_\Delta^2 Tr(\Delta^\dagger \Delta) + [\mu (H^{\rm T} i\sigma_2 \Delta^\dagger H) + \text{h.c.}] \\ & + \lambda_1 (H^\dagger H) Tr(\Delta^\dagger \Delta) + \lambda_2 (Tr \Delta^\dagger \Delta)^2 + \lambda_3 Tr(\Delta^\dagger \Delta)^2 + \lambda_4 H^\dagger \Delta \Delta^\dagger H \end{aligned} \tag{2.5}$$

where Tr is the trace over 2×2 matrices. $\mathcal{L}_{\rm Yukawa}$ contains on top of the Yukawa sector of the SM the extra term

$$-\, L^{\rm T} Y_\nu \otimes C \otimes i\sigma_2 \Delta L + \text{h.c.} \subset \mathcal{L}_{\rm Yukawa} \tag{2.6}$$

where L denotes the $SU(2)_L$ doublets of the left-handed leptons, Y_ν denotes a 3×3 matrix of Yukawa couplings in the lepton flavor space, suppressing flavor indices for simplicity, C the

[2] It has become customary in the literature to dub this model HTM or DTHM when focusing exclusively on the scalar sector. We will however stick here to the original name as the coupling to fermions will be of an issue in our study.

charge conjugation operator, and σ_2 the second Pauli matrix. The tensor product stresses the fact that these operators act on different spaces. In this paper we assume Y_ν to be diagonal, ignoring possible lepton flavor violation that could originate from the above term.

The spontaneous electroweak symmetry breaking is triggered by the structure of the minima of $V(H,\Delta)$ in the ten dimensional space of real valued scalar fields Eq.(2.1). The physically interesting minimum will correspond to non-zero vacuum expectation values v_d and v_t respectively for H and Δ along electrically neutral directions with $v_d \gg v_t$, such that the electroweak scale, $\sqrt{v_d^2+2v_t^2} \equiv 246\text{GeV}$, is given essentially by v_d while v_t induces neutrino Majorana masses through the Yukawa coupling Eq.(2.6). At the tree-level, the *necessary* electroweak symmetry breaking conditions read

$$M_\Delta^2 = \frac{2\mu v_d^2 - \sqrt{2}(\lambda_1+\lambda_4)v_d^2 v_t - 2\sqrt{2}(\lambda_2+\lambda_3)v_t^3}{2\sqrt{2}v_t} \tag{2.7}$$

$$m_H^2 = \frac{\lambda v_d^2}{4} - \sqrt{2}\mu v_t + \frac{(\lambda_1+\lambda_4)}{2}v_t^2 \tag{2.8}$$

We are not interested here in fine-tuning issues related to these equations when requiring $v_t \ll v_d$ in order to cope with the neutrino masses. We only note here that the regimes $M_\Delta \sim \mu \gg v_d$ or $\mu \ll v_t$ would not require fine-tuning. The first leads to a seesaw effect but to a BSM sector totally out of reach at the LHC, while the second does not feature a seesaw effect but is naturally compatible with neutrino masses and implies electroweak scale BSM physics.

After electroweak symmetry breaking the 10 scalar states decompose into 7 massive physical Higgses, $h^0, H^0, A^0, H^\pm, H^{\pm\pm}$ and 3 Goldstone bosons, with 3 angles α, β, β' mixing the neutral and singly charged doublet and triplet states,

$$h^0 = \cos\alpha\, h + \sin\alpha\, \xi^0, \qquad H^0 = -\sin\alpha\, h + \cos\alpha\, \xi^0 \tag{2.9}$$

$$A^0 = -\sin\beta\, Z_1 + \cos\beta\, Z_2, \qquad G^0 = \cos\beta\, Z_1 + \sin\beta\, Z_2 \tag{2.10}$$

$$G^\pm = \cos\beta'\phi^\pm + \sin\beta'\delta^\pm, \qquad H^\pm = -\sin\beta'\phi^\pm + \cos\beta'\delta^\pm \tag{2.11}$$

$$H^{\pm\pm} = \delta^{\pm\pm} \tag{2.12}$$

with the definitions $\phi^0 = \frac{1}{\sqrt{2}}(v_d + h + iZ_1), \delta^0 = \frac{1}{\sqrt{2}}(v_t + \xi^0 + iZ_2)$. Hereafter we make some general comments and then focus on the features directly related to the scenario under consideration. [For more details about the Higgs spectrum and couplings the reader

may refer to [22], [15].] The large hierarchy between v_d and v_t implies that $\sin\beta$ and $\sin\beta'$ in Eqs.(2.10, 2.11) are always suppressed, that is A^0 and $H^\pm$ carry essentially triplet components while the neutral and charged Goldstone bosons are essentially parts of the doublet. In contrast, $\sin\alpha$ scans all possible values but is either close to 0 or close to ± 1, apart from a fine-tuned region with maximal mixing $\sin\alpha \simeq 1/\sqrt{2}$, again due to the smallness of v_t/v_d. As a consequence, one has generically two possibilities which we will dub '*$\mathcal{H}$-scenarios*':

h^0-scenario: the lighest CP-even state h^0 is SM-like ($\sin\alpha \simeq 0$); this occurs typically when

$$\mu \gtrsim \hat{\mu}'_{(\mp)} \equiv (\lambda - \frac{2(\lambda-\lambda_1-\lambda_4)}{2\mp\sqrt{12+2k}})\frac{v_t}{\sqrt{2}} + \mathcal{O}(\frac{v_t^3}{v_d^2}) \tag{2.13}$$

where $k > 0$ is defined implicitly through

$$\cos\alpha|_{\mu=\hat{\mu}'_{(\mp)}} = 1 - k\frac{v_t^2}{v_d^2} + \mathcal{O}(\frac{v_t^3}{v_d^3}) \tag{2.14}$$

H^0-scenario: the heaviest CP-state H^0 is SM-like ($|\sin\alpha| \simeq 1$); this occurs typically when

$$0 < \mu \lesssim \hat{\mu}_{(\pm)} \equiv (\frac{\lambda}{\sqrt{2}} - \frac{\lambda-\lambda_1-\lambda_4}{\sqrt{2}\pm\sqrt{k}})v_t + \mathcal{O}(\frac{v_t^3}{v_d^2}) \tag{2.15}$$

where $k > 0$ is defined implicitly through

$$|\sin\alpha|_{\mu=\hat{\mu}_{(\pm)}} = 1 - k\frac{v_t^2}{v_d^2} + \mathcal{O}(\frac{v_t^3}{v_d^3}) \tag{2.16}$$

The upper bound in Eq.(2.15) has been derived in [15] to which we refer the reader for more details, while the bound in Eq.(2.13) is new.[3] As can be seen from Eqs.(2.14, 2.16), k parameterizes the purity of the SM-like Higgs state in both scenarios; for $k = 0$ all the couplings of the $\mathcal{H}$ state are strictly those of the SM. Phenomenologically, $\delta \equiv kv_t^2/v_d^2$ can be identified with a given precision at which the SM couplings are measured. It is readily related to the general effective parameterization [23]. Thus $\hat{\mu}$ and $\hat{\mu}'$ determine the domains of $v_t, \mu, \lambda, \lambda_1+\lambda_4$ that will not be excluded by merely narrowing down the experimental

[3] In both cases, the symbols $\pm$ and $\mp$ correspond to the sign of $\lambda-\lambda_1-\lambda_4$ and select the relevant (sufficient and necessary) bound to be used depending on this sign. In particular, this implies that the relevant bounds always satisfy $\hat{\mu} \lesssim \frac{\lambda}{\sqrt{2}}v_t \lesssim \hat{\mu}'$.

determination of the couplings, should they remain consistent with the SM within a given projected precision, [24],[25]. In fact, given the suppression factor v_t^2/v_d^2, it is only for very high precision, consistent with $k \sim \mathcal{O}(1)$, that $\hat{\mu}$ and $\hat{\mu}'$ become explicitly sensitive to v_t and $\lambda_1 + \lambda_4$, c.f. Eqs .(2.13, 2.15). This sensitivity is quickly lost for a precision δ of order a few percent. An implicit dependence on v_t and $\lambda_1 + \lambda_4$ will remain, however, in λ itself, when $m_{\mathcal{H}}$ is fixed at its observed value. For instance, in the H^0-*scenario* it will be given by Eq.(2.23).

We discuss now a little further some qualitative features of the two scenarios:

- in the h^0-*scenario* the new scalar states are of the same order or heavier than the SM-like Higgs state. The SM tree-level predictions *in the SM sector* are then generically only slightly modified. Signatures of the model can then come only from direct evidence for the new scalar states including the doubly charged one, together with evidence for Majorana neutrino masses and lepton number violating processes. However, the rationale for a seesaw mechanism operates strictly speaking when M_Δ and μ are assumed to have high scale (perhaps GUT scale) origin, leading to $\mu \sim M_\Delta \gg \mathcal{O}(1)$TeV. The case of such very large $\mu(\sim M_\Delta \sim M_{\rm GUT})$ is however of no relevance if one is interested at all in testable Higgs phenomenology at the colliders, since all the non-standard Higgs states decouple from the low energy (TeV) sector. In fact, taking $\mu \gtrsim \mathcal{O}(20)\, v_t$ for typical values of the λ_i's, already leads to states heavier than $\mathcal{O}(1)$ TeV and virtually out of reach at the LHC![4]

- in the H^0-*scenario* the $H^\pm$ and $H^{\pm\pm}$ masses are bounded from above disfavoring configurations with $\lambda_1 + \lambda_4 - \lambda < 0$ in order to cope with the present experimental lower bounds on these masses. Furthermore, the h^0 and A^0 states are lighter than the SM-like Higgs state and their masses will decrease with decreasing μ; the ensuing phenomenological issues will be addressed in section V. Here we comment on the plausibility of this $\mu \sim v_t$ or $\ll v_t$ scenario from the model-building point of view.

  As stated in the introduction, the relative magnitude of μ and v_t can be related to

[4] It is to be noted that even in this case low energy precision observables are not trivially consistent with the SM predictions. For instance deviation of the ρ-parameter from its SM tree- level value, $\rho \approx 1 - 2v_t/v_d < 1$, requires non-standard contributions to the radiative corrections in order to restore $\rho \gtrsim 1$ to reach consistency with the experimental value [26], [27] .

the status of the UV origin of lepton number conservation whose violation at the electroweak scale is triggered by these two parameters independently. Examples of scenarios where small μ is generated through one-loop suppressed effective operator, have been given in non-supersymmetric [28] or supersymmetric [29] extensions of the *type II seesaw* Lagrangian Eqs. (2.2 – 2.5). Although different, these scenarios have in common the assumption that μ triggers non-vanishing v_t, leading typically to $v_t \sim \mathcal{O}(\mu)$. However, the latter assumption is not necessary and in fact does not fully account for the general structure of the scalar potential Eq. (2.5); as one can see from Eqs.(2.7, 2.8), there are also μ independent contributions from the dimensionless couplings between H and Δ, mainly through the combination $\lambda_1 + \lambda_4$, so that the relative size μ/v_t can be much smaller than $\mathcal{O}(1)$ and still remain consistent with electroweak symmetry breaking. Furthermore, the loop suppressed mechanisms of [28] and [29] can operate even in this context.

Before ending this discussion we sketch yet another possibility, namely that lepton number violation be seeded by gravitational effects. We note first that the μ parameter is natural in the sense that putting it to zero increases the symmetry of the Lagrangian Eq. (2.2) [that is to a *global* $U(1)$ symmetry associated with the lepton number with charge assignments $l_\Delta = -2$, $l_H = 0$, $l_l = -l_{\bar{l}} = 1, l_q = l_{\bar{q}} = 0$]. A corollary is that a small μ remains small against radiative corrections before any spontaneous symmetry breaking, since as can be seen from Eq. (2.5) loop corrections to the operator "$H^{\mathrm{T}}\Delta^\dagger H$" will be proportional to μ itself. These properties are preserved in extensions of the model to larger gauge groups where H and Δ would be parts of some multiplets Φ and Σ respectively in the fundamental and adjoint representations of this gauge group. One can thus require consistently the conservation of the lepton number at the Lagrangian level, and this symmetry will be exactly preserved in the full theory, as far as energy scales above the spontaneous breaking of some of the gauge symmetries are concerned. However, this global symmetry is expected to be broken when (quantum) gravitational effects are switched on (see [30] for a recent reappraisal). This breaking would manifest itself at scales lower than the Planck scale M_{Pl}, through the presence of higher dimensional operators suppressed by powers of M_{Pl}. The leading effect originates from the dimension-5 gauge invariant and lepton number violating operator, $\Phi^\dagger\Phi(\Phi^{\mathrm{T}}\Sigma^\dagger\Phi)$ (where we suppressed the group indices for simplicity). An effective μ

parameter of order $\langle\Phi\rangle^2/M_{Pl}$ will thus be generated at an intermediate scale where spontaneous breaking of (some of) the gauge symmetries takes place, triggered by the vacuum expectation value of the field Φ. This mechanism has two nice features –for one thing, it relates the magnitude of μ to the scale at which the underlying gauge symmetry is broken; obviously $\langle\Phi\rangle \sim O(M_{GUT})$ leads back to h^0-*scenario*, while assuming a desert between the electroweak and the Planck scales leads to a μ of order $10^{-14} - 10^{-15}$GeV at the edge of the phenomenologically acceptable values in H^0-*scenario* –for the other, by choosing $246\text{GeV} \ll \langle\Phi\rangle \ll M_{GUT}$ one can arrange to have all the extended sector too heavy to be accessible to the colliders but still keeping μ very small independently of the value of v_t. We do not dwell further here on an explicit building of the model which is out of the scope of the present paper. We only take the above general arguments as a motivation to study the phenomenology of configurations satisfying $\mu/v_t \ll 1$.

When dealing with the H^0-*scenario* it will be instructive to expand the various scalar field masses in terms of the small ratio μ/v_t. Starting from the exact tree-level expressions [15], one finds,

$$m^2_{h^0} = 2\,(\lambda^+_{23} - \frac{(\lambda^+_{14})^2}{\lambda})\,v_t^2 + \frac{1}{\sqrt{2}}\frac{\mu}{v_t}\,(v_d^2 + 4\,(2\,\lambda - \lambda^+_{14})\,\lambda^+_{14}\,\frac{v_t^2}{\lambda^2}) + \mathcal{O}(\frac{\mu^2}{v_t^2}) \tag{2.17}$$

$$m^2_{H^0} = \lambda\,\frac{v_d^2}{2} + 2\,\frac{(\lambda^+_{14})^2}{\lambda}\,v_t^2 - 2\sqrt{2}\,\frac{\mu}{v_t}\,(2\,\lambda - \lambda^+_{14})\,\lambda^+_{14}\,\frac{v_t^2}{\lambda^2} + \mathcal{O}(\frac{\mu^2}{v_t^2}) \tag{2.18}$$

$$m^2_{A^0} = \frac{1}{\sqrt{2}}\frac{\mu}{v_t}\,(v_d^2 + 4\,v_t^2) \tag{2.19}$$

$$m^2_{H^+} = (-\frac{\lambda_4}{4} + \frac{1}{\sqrt{2}}\frac{\mu}{v_t})\,(v_d^2 + 2\,v_t^2) + \mathcal{O}(\frac{\mu^2}{v_t^2}) \tag{2.20}$$

$$m^2_{H^{++}} = -\lambda_4\,\frac{v_d^2}{2} - \lambda_3\,v_t^2 + \frac{\mu}{v_t}\,\frac{v_d^2}{\sqrt{2}} + \mathcal{O}(\frac{\mu^2}{v_t^2}) \tag{2.21}$$

where we used the shorthand notation $\lambda^+_{14} \equiv \lambda_1 + \lambda_4$, $\lambda^+_{23} \equiv \lambda_2 + \lambda_3$, and kept negligible v_t^2 contributions in order to assess small splitting as well as no-tachyon conditions.

The splitting $\Delta m_0^2 \equiv m^2_{h^0} - m^2_{A^0}$ verifies,

$$\Delta m_0^2 \leq 2\,(\lambda_2 + \lambda_3 - \sqrt{2}\,\frac{\mu}{v_t})\,v_t^2 + \mathcal{O}(\frac{\mu^2}{v_t^2}) \tag{2.22}$$

and thus remains very small as compared to the allowed values of m_{h^0} and m_{A^0} (see section V), even for the largest allowed values of $v_t(\sim 1GeV)$ and $(\lambda_2 + \lambda_3)|_{\max} = \kappa\frac{\pi}{5} \approx 5$ (see the

discussion in appendix B and [15]). In the sequel we will always assume $m_{h^0} \simeq m_{A^0}$. Note also that the exact form for m_{A^0} comes naturally proportional to μ/v_t. This is reminiscent of the would-be-Goldstone character of A^0 in the limit $\mu \to 0$, $v_t \neq 0$ of spontaneous breaking of the continuous lepton number symmetry. It stresses as well the fact that the magnitude of m_{A^0} is not controlled solely by μ, but also by v_t as two independent parameters.

As can be seen from Eq. (2.17), one retrieves consistently an approximate lower bound on μ that ensures a non-tachyonic h^0 (see [15] for the exact bounds). Also this bound evaporates if $\lambda_{23}^+ - \frac{(\lambda_{14}^+)^2}{\lambda} > 0$, the latter being consistent with a bounded from below potential, see appendix B. In any case, the no-tachyon issue is independent of the sign of of λ_{14}^+, thus illustrating the fact that $M_\Delta^2 < 0$, c.f. Eq. (2.7), is perfectly compatible with consistent electroweak symmetry breaking, contrary to what is sometimes stated in the literature. Even more so, for $\mu \ll v_t$, requiring $M_\Delta^2 > 0$ boils down to requiring $\lambda_{14}^+ < 0$ which in turn excludes the *H^0-scenario* altogether for any value of $\mu(> 0)$ in the strict SM-like limit with $k = 0$, c.f. Eq. (2.15). Put differently, insisting on $M_\Delta^2 > 0$ excludes *a priori* a viable scenario rather than non-physical configurations! Obviously another no-tachyon constraint will be $\lambda_4 < 0$ as can be seen from Eqs. (2.20, 2.21). The discussion of the more stringent experimental exclusion constraints is deferred to the subsequent sections.

Finally, inverting Eq.(2.18) one obtains

$$\lambda = \frac{2m_{H^0}^2}{v_d^2} - \frac{\lambda_{14}^+ v_t^2}{m_{H^0}^2}\,(2\lambda_{14}^+ + \sqrt{2}\,(\lambda_{14}^+ \frac{v_d^2}{m_{H^0}^2} - 4)\,\frac{\mu}{v_t}) + \mathcal{O}(\frac{\mu^2}{v_t^2}) \tag{2.23}$$

which gives the precise correlation of λ with the other parameters of the model for fixed m_{H^0}. In practice this relation will be useful for consistent scans keeping the SM-Higgs-like scalar mass at it's experimentally measured value within $\mathcal{O}(1)$GeV precision.

We end this section by recalling the mixing angles and various couplings of the model that will be relevant for the phenomenological study in the rest of the paper.

mixing angles: using the shorthand notations s_x, c_x for $\cos x, \sin x$, the angles β and β' are given by

$$s_\beta = \frac{2v_t}{\sqrt{v_d^2 + 4v_t^2}}\,, \qquad c_\beta = \frac{v_d}{\sqrt{v_d^2 + 4v_t^2}} \tag{2.24}$$

$$s_{\beta'} = \frac{\sqrt{2}v_t}{\sqrt{v_d^2 + 2v_t^2}} \qquad , \qquad c_{\beta'} = \frac{v_d}{\sqrt{v_d^2 + 2v_t^2}} \tag{2.25}$$

up to an arbitrary global sign (but the same for s_x and c_x) independently of the considered $\mathcal{H}$-*scenario*. The expressions for the mixing angle α are more involved (see [15]). We give them here for simplicity in the limits $\mu \to \infty$ and $\mu \to 0$, illustrating two special cases of respectively the h^0-, H^0-*scenarios*,

$\mu \to \infty$:

$$s_\alpha \;=\; \frac{\bar{\epsilon}}{\sqrt{2}}\sqrt{1-\frac{v_d}{\sqrt{v_d^2+16v_t^2}}} \approx 2\frac{v_t}{v_d}+\mathcal{O}(\frac{v_t^3}{v_d^3}), \quad c_\alpha = \sqrt{\frac{1}{2}+\frac{v_d}{2\sqrt{v_d^2+16v_t^2}}} \approx 1 \tag{2.26}$$

$\mu \to 0$:

$$s_\alpha \;=\; \bar{\epsilon}(1-2\frac{{\lambda_{14}^+}^2}{\lambda^2}\frac{v_t^2}{v_d^2})+\mathcal{O}(\frac{v_t^3}{v_d^3}), \qquad\qquad c_\alpha = 2\frac{|\lambda_{14}^+|}{\lambda}\frac{v_t}{v_d}+\mathcal{O}(\frac{v_t^3}{v_d^3}) \tag{2.27}$$

where, adopting the convention $c_\alpha > 0$, the sign $\bar{\epsilon}$ is given by

$$\bar{\epsilon}=1,\ [h^0\text{-}scenario] \qquad , \qquad \bar{\epsilon}=\text{sign}[\sqrt{2}\mu-(\lambda_1+\lambda_4)v_t],\ [H^0\text{-}scenario] \tag{2.28}$$

In the following and throughout the paper we refer to the couplings as they appear in the Lagrangian, [i.e. no extra i factors or symmetry factors of Feynman rules]:

gauge boson(-gauge boson)-scalar-(scalar) couplings: it is easy to see from the structure of the kinetic terms Eqs. (2.2 – 2.4) and the scalar field components that develop vacuum expectation values, that couplings involving one scalar boson and two gauge bosons are v_t suppressed if the scalar is essentially triplet; couplings involving one or two gauge bosons and two scalars are v_t suppressed only if one of the scalars is triplet-like and the other doublet-like; all other cases feature SM-like couplings. For instance the magnitudes of the derivative couplings $Z^0h^0A^0, Z^0H^0A^0$ are $\mathcal{H}$-*scenario* dependent and read (skipping the Lorentz structure for simplicity):

$$g_{Z^0h^0A^0} = -\frac{g}{2c_W}(c_\alpha s_\beta - 2c_\beta s_\alpha) \;\approx \frac{g}{c_W}\frac{v_t}{v_d}(2\bar{\epsilon}-1),\ [h^0\text{-}scenario];\ \approx \bar{\epsilon}\frac{g}{c_W},\ [H^0\text{-}scenario] \tag{2.29}$$

$$g_{Z^0H^0A^0} = \frac{g}{2c_W}(s_\alpha s_\beta + 2c_\alpha c_\beta) \;\approx \frac{g}{c_W},\ [h^0\text{-}scenario];\ \approx \frac{g}{c_W}\frac{v_t}{v_d}(\bar{\epsilon}+2\frac{|\lambda_{14}^+|}{\lambda}),\ [H^0\text{-}scenario] \tag{2.30}$$

while the magnitudes of the Z-boson to the (doubly-)charged Higgs bosons derivative couplings are $\mathcal{H}$-*scenario* independent and given by

$$g_{ZH^+H^-} \;=\; +\frac{1}{2}[-(c_W^2\, s_{\beta'}^2)+(2c_{\beta'}^2+s_{\beta'}^2)\, s_W^2]/(s_W\, c_W) \approx s_W/c_W \tag{2.31}$$

$$g_{ZH^{++}H^{--}} \;=\; -[c_W^2-s_W^2]/(s_W\, c_W) = -2\cot 2\theta_W \tag{2.32}$$

[Note that Eq.(2.31) differs from the one given in our Eq.(C.20) of ref.[15], due to a typo in the latter.] The γH^+H^- and $\gamma H^{++}H^{--}$ couplings are obviously those of (scalar) QED and are given by the H^+ and H^{++} electric charges.

triple-scalar couplings: again, one easily sees from the structure of the potential Eq. (2.5) and the vacuum expectation values, that triple scalar couplings are v_t suppressed when only one of the three scalars is triplet-like, and not suppressed when only one of the three scalars is doublet-like. For instance the couplings $h^0h^0H^0$, $A^0A^0H^0$, $h^0H^{++}H^{--}, h^0H^+H^-, H^0H^{++}H^{--}, H^0H^+H^-$ are given by

$$g_{h^0h^0H^0} = \sqrt{2}c_\alpha\mu(1-3s_\alpha^2) + (\frac{3}{2}c_\alpha^2\lambda + (1-3c_\alpha^2)\lambda_{14}^+)s_\alpha v_d - c_\alpha(6\lambda_{23}^+ s_\alpha^2 + \lambda_{14}^+(1-3s_\alpha^2))v_t \quad (2.33)$$

$$g_{A^0A^0H^0} = \sqrt{2}\,\mu\, s_\beta\,(2\,c_\beta\, s_\alpha - c_\alpha\, s_\beta) + s_\alpha\,(c_\beta^2\,\lambda_{14}^+ + \frac{\lambda}{2}\,s_\beta^2)v_d - c_\alpha(2\,c_\beta^2\,\lambda_{23}^+ + \lambda_{14}^+\,s_\beta^2)v_t\,(2.34)$$

$$\begin{aligned} g_{h^0H^{++}H^{--}} &= -\{2\lambda_2 v_t s_\alpha + \lambda_1 v_d c_\alpha\} && (2.35)\\ g_{h^0H^+H^-} &= -\frac{1}{2}\Big\{\{4v_t(\lambda_2+\lambda_3)c_{\beta'}^2 + 2v_t\lambda_1 s_{\beta'}^2 - \sqrt{2}\lambda_4 v_d c_{\beta'}s_{\beta'}\}s_\alpha \\ &\quad +\{\lambda\, v_d s_{\beta'}^2 + (2\lambda_1+\lambda_4)v_d c_{\beta'}^2 + (4\mu - \sqrt{2}\lambda_4 v_t)c_{\beta'}s_{\beta'}\}c_\alpha\Big\} && (2.36)\end{aligned}$$

and

$$\begin{aligned} g_{H^0H^{++}H^{--}} &= g_{h^0H^{++}H^{--}}[c_\alpha \to -s_\alpha, s_\alpha \to c_\alpha] && (2.37)\\ g_{H^0H^+H^-} &= g_{h^0H^+H^-}[c_\alpha \to -s_\alpha, s_\alpha \to c_\alpha] && (2.38)\end{aligned}$$

These couplings are phenomenologically interesting in both h^0-, H^0-*scenarios*. In the former they will trigger decays of the heavy non-standard CP-even state. In the latter they will trigger non-standard decays of the SM-Higgs-like state. The couplings to (doubly-)charged states will be important in both $\mathcal{H}$-*scenarios* when studying the $\gamma\gamma$ and $Z\gamma$ Higgs decay channels. We give in table I the limiting behavior for all these couplings in the two $\mathcal{H}$-*scenarios* for later reference.

Yukawa couplings: it is straightforward to obtain these couplings from the Yukawa sector of the SM and the extra Yukawa terms Eq. (2.6), upon use of Eqs. (2.9 –2.12). For instance the $A^0\bar{f}f$ and $H^\pm\bar{f}'f$ couplings are given by the corresponding SM neutral and charged Goldstone bosons, suppressed respectively by $-\sin\beta$, and $-\sin\beta'$. Similarly, the $h^0\bar{f}f$,

$\approx$	h^0-*scenario*	H^0-*scenario*
$g_{h^0h^0H^0}$	$\sqrt{2}\mu - (5\lambda_{14}^+ - 3\lambda)v_t$	$\bar{\epsilon}\lambda_{14}^+ v_d$
$g_{A^0A^0H^0}$	$2(\lambda_{14}^+ - \lambda_{23}^+)v_t + 4\sqrt{2}\mu\frac{v_t^2}{v_d^2}$	$\bar{\epsilon}\lambda_{14}^+ v_d$
$g_{h^0H^{++}H^{--}}$	$-\lambda_1 v_d$	$-2(\bar{\epsilon}\lambda_2 + \lambda_1\frac{\lvert\lambda_{14}^+\rvert}{\lambda})v_t$
$g_{h^0H^+H^-}$	$-(\lambda_1 + \frac{\lambda_4}{2})v_d - 2\sqrt{2}\mu\frac{v_t}{v_d}$	$(-2(\frac{\lambda_{14}^+\lvert\lambda_{14}^+\rvert}{\lambda} + \bar{\epsilon}\lambda_{23}^+) + (\bar{\epsilon} + \frac{\lvert\lambda_{14}^+\rvert}{\lambda})\lambda_4)v_t$
$g_{H^0H^{++}H^{--}}$	$2(\lambda_1 - \lambda_2)v_t$	$\bar{\epsilon}\lambda_1 v_d$
$g_{H^0H^+H^-}$	$2v_t(\lambda_{14}^+ - \lambda_{23}^+) + 4\sqrt{2}\mu\frac{v_t^2}{v_d^2}$	$\bar{\epsilon}(\lambda_1 + \frac{\lambda_4}{2})v_d$

TABLE I: Approximate expressions in the h^0-, H^0-*scenarios*, for a selected list of three-scalar couplings as they appear in the Lagrangian.

$H^0\bar{f}f$ couplings are given by the SM Higgs coupling to fermions suppressed respectively by $\cos\alpha$ and $-\sin\alpha$. Also charge conservation forbids $H^{\pm\pm}$ from inheriting from any of the SM Yukawa couplings. Taking into account Eqs. (2.24 – 2.27), one retrieves that all the new scalar states become increasingly fermiophobic with decreasing v_t, except for one CP-even state that becomes increasingly SM-like. In contrast, the new Yukawa terms of Eq.(2.6) induce couplings of the scalar states, through their triplet components, to same lepton number lepton and neutrino pairs. All these coupings are proportional to $(Y_\nu)_l \equiv m_{\nu_l}/\sqrt{2}v_t$, (we take for simplicity here diagonal flavor-conserving Y_ν matrix), and the mixing to the triplet components are not suppressed except for the SM-Higgs-like state, c.f. Eqs. (2.9 – 2.12, 2.24 – 2.27). Thus all the new scalar states become increasingly 'same-lepton-number-philic' with decreasing v_t, excepted the SM-Higgs-like state whose coupling to pairs of (anti-)neutrinos is $\mathcal{O}(m_{\nu_l}/v_d)$ suppressed as can be seen from s_α, Eq.(2.26), and c_α, Eq.(2.27). We give the magnitudes of these couplings in table II. [An extended list of couplings can be found elsewhere in the literature; see for instance the appendix of [15] and [22], albeit with different notations in the latter. We note however a disagreement in the relative sign in the $H^+\bar{f}'f$ coupling given in table II as compared to the one given in Table VII of ref.[22].]

$\approx$	h^0-*scenario*/H^0-*scenario*
$g_{h^0\bar{f}f}$	$-\frac{m_f}{v_d}$ / $-2\frac{\lvert\lambda_{14}^+\rvert}{\lambda}\frac{m_f v_t}{v_d^2}$
$g_{H^0\bar{f}f}$	$-2\frac{m_f v_t}{v_d^2}$ / $-\bar{\epsilon}\frac{m_f}{v_d}$
$g_{A^0\bar{f}f}$	$2i\frac{m_f v_t}{v_d^2}\gamma_5$
$g_{H^+\bar{f}'f}$	$-2\frac{v_t}{v_d^2}(m_{f'}P_L - m_f P_R)$
$g_{h^0\nu_l\nu_l(\bar{\nu}_l\bar{\nu}_l)}$	$-\frac{m_{\nu_l}}{v_d}CP_L$ / $-\bar{\epsilon}\frac{m_{\nu_l}}{2v_t}CP_L$
$g_{H^0\nu_l\nu_l(\bar{\nu}_l\bar{\nu}_l)}$	$-\frac{m_{\nu_l}}{2v_t}CP_L$ / $-\frac{\lvert\lambda_{14}^+\rvert}{\lambda}\frac{m_{\nu_l}}{v_d}CP_L$
$g_{A^0\nu_l\nu_l(\bar{\nu}_l\bar{\nu}_l)}$	$-i\frac{m_{\nu_l}}{2v_t}CP_L$
$g_{H^+l^-\nu_l}$	$\frac{m_{\nu_l}}{v_t}CP_L$
$g_{H^{++}l^-l^-}$	$\frac{m_{\nu_l}}{\sqrt{2}v_t}CP_L$

TABLE II: The Yukawa couplings as they appear in the Lagrangian after electroweak symmetry breaking. P_L, P_R denote the left,right chirality projectors, and we have substituted the values of the various mixing angles, in the h^0-, H^0-*scenarios*. The upper (resp. lower) block corresponds to the operators involving opposite (resp. same) lepton-number fermions.

III. $\mathcal{H} \to \gamma\gamma, Z\gamma$

In this section we study the effects of the *type II seesaw* model on the diphoton and $Z\gamma$ decay channels of the SM-Higgs-like scalar. These channels have been considered in the literature in various BSM scenarios as they can probe new heavy degrees of freedom through loop effects. In the *type II seesaw* they probe the presence of the $H^\pm$ and $H^{\pm\pm}$ states as well as non-zero coupling between the doublet and triplet scalar sectors. Note that in the model under consideration, the gluon fusion production channel remains essentially standard since the new states are not colored and, furthermore, the top and bottom quark Yukawa couplings are very close to SM-like in both $\mathcal{H}$- *scenarios*.

The relative tension between ATLAS [31] and CMS [32] regarding the diphoton channel has essentially evaporated [8, 9]. Anticipating that the future analyses with accumulated luminosity and increased C.M. energy at the LHC will confirm further the SM predictions for this channel, the $Z\gamma$ channel could still provide independent and complementary information on BSM physics. Hereafter, we first recall the theoretical structure of these two channels and then discuss their phenomenological features and correlations.

A. $\mathcal{H} \to \gamma\gamma$

The structure of the diphoton decay channel width in the *type II seesaw* model can be summarized as follows:

$$\begin{aligned}\Gamma(\mathcal{H}\to\gamma\gamma) \;=\; & \frac{G_F\alpha^2 M_{\mathcal{H}}^3}{128\sqrt{2}\pi^3}\Big|\sum_f N_c Q_f^2 \tilde{g}_{\mathcal{H}ff} A_{1/2}^{\mathcal{H}}(\tau_f) + \tilde{g}_{\mathcal{H}WW} A_1^{\mathcal{H}}(\tau_W) \\ & + Q_+^2 \tilde{g}_{\mathcal{H}H^+H^-} A_0^{\mathcal{H}}(\tau_{H^+}) + Q_{++}^2 \tilde{g}_{\mathcal{H}H^{++}H^{--}} A_0^{\mathcal{H}}(\tau_{H^{++}})\Big|^2 \end{aligned} \tag{3.1}$$

where we have introduced the units of electric charge of H^+ and H^{++}, namely $Q_+ = 1$ and $Q_{++} = 2$, for later use in the next section. The scalar functions $A_0^{\mathcal{H}}, A_{1/2}^{\mathcal{H}}$ and $A_1^{\mathcal{H}}$ corresponding to spin-$0, 1/2, 1$ contributions in the loops are defined as,

$$A_{1/2}^{\mathcal{H}}(\tau) \;=\; 2[\tau + (\tau-1)f(\tau)]\,\tau^{-2} \tag{3.2}$$

$$A_1^{\mathcal{H}}(\tau) \;=\; -[2\tau^2 + 3\tau + 3(2\tau-1)f(\tau)]\,\tau^{-2} \tag{3.3}$$

$$A_0^{\mathcal{H}}(\tau) \;=\; -[\tau - f(\tau)]\,\tau^{-2} \tag{3.4}$$

with $\tau_i = m_{\mathcal{H}}^2/4m_i^2$ $(i = f, W, H^+, H^{++})$ and the function $f(\tau)$ is given by

$$f(\tau) = \begin{cases} \arcsin^2\sqrt{\tau} & \tau \le 1 \\ -\dfrac{1}{4}\left[\log\dfrac{1+\sqrt{1-\tau^{-1}}}{1-\sqrt{1-\tau^{-1}}} - i\pi\right]^2 & \tau > 1 \end{cases} \tag{3.5}$$

while the *reduced* trilinear couplings of $\mathcal{H}$ to H^+ and H^{++} are given by

$$\tilde{g}_{\mathcal{H}H^{++}H^{--}} \;=\; -\frac{s_W}{e}\frac{m_W}{m_{H^{++}}^2} g_{\mathcal{H}H^{++}H^{--}} \tag{3.6}$$

$$\tilde{g}_{\mathcal{H}H^{+}H^{-}} \;=\; -\frac{s_W}{e}\frac{m_W}{m_{H^{+}}^2} g_{\mathcal{H}H^{+}H^{-}} \tag{3.7}$$

where $g_{\mathcal{H}H^{++}H^{--}}, g_{\mathcal{H}H^{+}H^{-}}$ can be found in table I for the corresponding $\mathcal{H}$-scenario. When $\mu v_t \ll v_d^2$, they can be summarized as

$$g_{\mathcal{H}H^{++}H^{--}} \approx -s\lambda_1 v_d \tag{3.8}$$

$$g_{\mathcal{H}H^{+}H^{-}} \approx -s(\lambda_1 + \frac{\lambda_4}{2})v_d \tag{3.9}$$

by defining $s = 1$ in the h^0-*scenario* ($\mathcal{H} \equiv h^0$), and $s = -\bar{\epsilon}$ in the H^0-*scenario* ($\mathcal{H} \equiv H^0$) with $\bar{\epsilon}$ as given by Eq.(2.28).[5]

$\mathcal{H}$	$\tilde{g}_{\mathcal{H}\bar{u}u}$	$\tilde{g}_{\mathcal{H}\bar{d}d}$	$\tilde{g}_{\mathcal{H}W^+W^-}$
h^0	$c_\alpha/c_{\beta'}$	$c_\alpha/c_{\beta'}$	$+e(c_\alpha\, v_d + 2s_\alpha\, v_t)/(2s_W\, m_W)$
H^0	$-s_\alpha/c_{\beta'}$	$-s_\alpha/c_{\beta'}$	$-e(s_\alpha\, v_d - 2c_\alpha\, v_t)/(2s_W\, m_W)$

TABLE III: The CP-even neutral Higgs *reduced* couplings to fermions and gauge bosons in the *type II seesaw* model relative to the SM Higgs couplings, α and β' denote the mixing angles respectively in the CP-even and charged Higgs sectors, e is the electron charge, m_W the W gauge boson mass and s_W the weak mixing angle.

B. $\mathcal{H} \to Z\gamma$

Since the original work [34], [35], various notations and normalizations have been adopted by different reviewers (see e.g. [36], [37], [38]) as well as by authors of very recent studies specific to the *type II seesaw* model [20], [39, 40] (not to mention different notational conventions for the scalar couplings in the *type II seesaw* model potential). This unfortunately makes comparisons among different forms for $\Gamma(\mathcal{H} \to Z\gamma)$ unnecessarily tedious and a direct use of the literature to include new loop contributions far from straightforward, leading occasionally to erroneous factors. We have thus recomputed $\Gamma(\mathcal{H} \to Z\gamma)$ from scratch, using the FeynArts and FormCalc [41, 42] packages for the one-loop amplitudes, for which we provided a *type II seesaw* model file. We then compared with [36], [37] and checked the

[5] Note an overall sign mismatch between Eq.(3.9) above and Eq.(3.16) of [33]. This is just due to a notational confusion between s and $\bar{\epsilon}$ in the latter paper, but which did not enter nor affect the physics analysis!

consistency of the different normalizations. In the form we give below, we adopt conventions that are natural in the following sense:

- the couplings are identified as the ones read directly from the Lagrangian (up to an electric charge factor e)
- the defined functions correspond directly to the loop form factors
- the partial width $\Gamma(\mathcal{H} \to \gamma\gamma)$ of Eq.(3.1) is obtained straightforwardly from $\Gamma(\mathcal{H} \to Z\gamma)$ in an appropriate formal limit with $M_Z \to 0$.

With these conventions we find,

$$\begin{aligned}\Gamma(\mathcal{H} \to Z\gamma) \;=\; & \frac{G_F^2 M_W^2\, \alpha\, M_{\mathcal{H}}^3}{64\,\pi^4}\left(1-\frac{M_Z^2}{M_{\mathcal{H}}^2}\right)^3 s_W^2 \Bigg| \sum_f N_c^f\, g_{\gamma ff} g_{Zff}^v\, \tilde{g}_{\mathcal{H}ff}\, A_{1/2}^{\mathcal{H}}(\tau_f,\lambda_f) \\ & + g_{\gamma WW} g_{ZWW} \tilde{g}_{\mathcal{H}WW}\, A_1^{\mathcal{H}}(\tau_W,\lambda_W) + Q_+ g_{ZH^+H^-} \tilde{g}_{\mathcal{H}H^+H^-}\, A_0^{\mathcal{H}}(\tau_{H^+},\lambda_{H^+}) \\ & + Q_{++} g_{ZH^{++}H^{--}} \tilde{g}_{\mathcal{H}H^{++}H^{--}}\, A_0^{\mathcal{H}}(\tau_{H^{++}},\lambda_{H^{++}})\Bigg|^2 \end{aligned} \tag{3.10}$$

where τ_i is defined as in section III A and $\lambda_i = M_Z^2/4m_i^2$ $(i = f, W, H^+, H^{++})$, $g_{Zff}^v = -\frac{(I_f^3 - 2s_W^2 Q_f)}{2 s_W c_W}$, with Q_f denoting the fermions electric charges and I_f their weak isospin, $g_{\gamma ff} = -Q_f$, $g_{ZWW} = -\cot\theta_W$, $g_{\gamma WW} = -1$ and

$$A_{1/2}^{\mathcal{H}}(\tau,\lambda) \;=\; -4\,[I_1(\tau,\lambda) - I_2(\tau,\lambda)] \tag{3.11}$$

$$A_1^{\mathcal{H}}(\tau,\lambda) \;=\; 2\,\{[2(1+2\tau)(1-\lambda) + (1-2\tau)]I_1(\tau,\lambda) - 8(1-\lambda)I_2(\tau,\lambda)\} \tag{3.12}$$

$$A_0^{\mathcal{H}}(\tau,\lambda) \;=\; 2I_1(\tau,\lambda) \tag{3.13}$$

The functions I_1 and I_2 are given by

$$\begin{aligned} I_1(\tau,\lambda) \;&=\; \frac{1}{2(\lambda-\tau)} + \frac{1}{2(\tau-\lambda)^2}\,[f(\tau) - f(\lambda)] + \frac{\lambda}{(\tau-\lambda)^2}\,[g(\tau) - g(\lambda)] \\ I_2(\tau,\lambda) \;&=\; \frac{1}{2(\tau-\lambda)}\,[f(\tau) - f(\lambda)] \end{aligned} \tag{3.14}$$

where $f(\tau)$ is given in Eq.(3.5)and $g(\tau)$ is defined as

$$g(\tau) = \begin{cases} \sqrt{\tau^{-1}-1}\,\arcsin\sqrt{\tau} & \tau \le 1 \\ \dfrac{\sqrt{1-\tau^{-1}}}{2}\left[\log\dfrac{1+\sqrt{1-\tau^{-1}}}{1-\sqrt{1-\tau^{-1}}} - i\pi\right] & \tau > 1 \end{cases} \tag{3.15}$$

The *reduced* couplings $\tilde{g}_{\mathcal{H}ff}, \tilde{g}_{\mathcal{H}WW}, \tilde{g}_{\mathcal{H}H^+H^-}$ and $\tilde{g}_{\mathcal{H}H^{++}H^{--}}$ are as given in table (III) and Eqs.(3.6 - 3.9). The $g_{ZH^+H^-}$, $g_{ZH^{++}H^{--}}$ couplings are given in Eqs. (2.31, 2.32). We adopted for the definition of $A_1^{\mathcal{H}}$ that of eq.(3.12), see also [39], rather than the more often used one,

$$A_1^{\mathcal{H}}(\tau_W, \lambda_W) = -\left\{4\left(3 - \frac{s_W^2}{c_W^2}\right) I_2(\tau_W, \lambda_W) + \left[(1+2\tau_W)\,\frac{s_W^2}{c_W^2} - (5+2\tau_W)\right] I_1(\tau_W, \lambda_W)\right\} \tag{3.16}$$

Both coincide only when the W-boson is circulating in the loop and upon use of the tree-level relation $M_W^2 = c_W^2 M_Z^2$. Eq. (3.12) is obviously more transparent if one wishes to include effects of heavier new gauge bosons, or for that matter to retrieve the diphoton channel by simply taking $\lambda \to 0$.[6] Note also that with our conventions the amplitude in Eq.(3.10) has a global minus sign as compared to [37].

C. Correlations

Hereafter we examine some model-dependent properties of the $\mathcal{H} \to \gamma\gamma, Z\gamma$ branching ratios as well as the correlation between the two channels.

The behavior of the branching ratio $\mathrm{Br}(\mathcal{H} \to \gamma\gamma)$ has already been studied in [33], (see also [27], [16] and the discussion in section IV). Here we discuss this behavior in somewhat more details taking into account the realistic $m_{\mathcal{H}} = 125-126$GeV mass. The main message is that, for not too heavy H^{++} and H^+, the virtual effects of these states bring in a high sensitivity to λ_1 and λ_{14}^+, (on top of an implicit sensitivity to λ_4 through the H^{++}, H^+ masses themselves). The quadratic dependence on λ_1 implies generically the existence of two-fold (λ_1, λ_4) values that are compatible with the SM prediction for $\mathrm{Br}(\mathcal{H} \to \gamma\gamma)$; that is, for any given value of λ_4, the branching ratio as a function of λ_1 crosses twice the SM value, once for λ_1 very close to zero and once for λ_1 of order a few units. This is of course a direct consequence of interference effects involving the (doubly)-charged scalars and the quasi-SM W and top-, bottom-quark loops. In fact, since λ_1, λ_4 are real-valued (see Eq.(2.5)), and taking into account that only the bottom-quark loop develops an absorptive imaginary contribution, a close look at the structure of Eq.(3.1) allows to trace the origin of small (resp. large) values of λ_1 compatible

[6] If Eq.(3.16) were to be used instead, then one would have to make the formal and unintuitive replacement $\frac{s_W^2}{c_W^2} \to -1$.

with the SM prediction of $\mathrm{Br}(\mathcal{H} \to \gamma\gamma)$, to a destructive interference in the H^+, H^{++} sector alone (resp. to a substantial interference between H^+, H^{++} and the W and top loops). Note that since present experimental constraints imply $m_{\mathcal{H}} < 2m_{H^+}, 2m_{H^{++}}$, the H^+, H^{++} loops do not have imaginary contributions (we are neglecting the widths of particles propagating in the loops), which would have otherwise destroyed the generic cancellations that we are discussing. We stress that none of these two (λ_1, λ_4) regions that are compatible with the SM prediction for $\mathrm{Br}(\mathcal{H} \to \gamma\gamma)$ correspond to any sort of decoupling regime. Indeed, they occur for moderate values of λ_4, hence for relatively light H^+, H^{++}. This means that the confirmation of a SM- like value for $\mathrm{Br}(\mathcal{H} \to \gamma\gamma)$ will not suffice by itself to exclude the existence of nearby new charged scalar states, nor even the possibility of relatively large λ_1, λ_4 values. One should however keep in mind that a consistent interpretation in terms of the h^0- or H^0-*scenarios* will bring a further constraint due to Eqs.(2.13, 2.15). Moreover, although we require the range of variation of (λ_1, λ_4) to respect the perturbative unitarity and boundedness from below (U-BFB) constraints (with $\kappa = 8$, see next section for a full discussion), still some values of λ_1 compatible with $\mathrm{Br}(\mathcal{H} \to \gamma\gamma)^{(\mathrm{SM})}$ can be relatively large, possibly questioning the validity of the perturbative evaluation. A more sophisticated treatment would be called for in this case, resumming for instance some of the higher order effects. We illustrate the above features in Figs.2 (a), (b) respectively in the h^0-*scenario* and H^0-*scenario* where we depicted also the SM model line. We allow conservatively a 10% uncertainty on the future determination of the SM Higgs couplings to fermions and gauge bosons, [24], [25]. This amounts to requiring $0.9 \leq c_\alpha \leq 1$, respectively $0.9 \leq |s_\alpha| \leq 1$, in the h^0-*scenario*, respectively H^0-*scenario*. Note that in terms of the κ-coupling scale factors [23], one has, depending on the h^0- or H^0-*scenario* under consideration, respectively $\kappa_F = c_\alpha$, or s_α, and $\kappa_Z = c_\alpha c_\beta + 2 s_\alpha s_\beta$ or $s_\alpha c_\beta - 2 c_\alpha s_\beta$, and $\kappa_W = c_\alpha c_\beta + s_\alpha s_\beta$ or $c_\alpha s_\beta - s_\alpha c_\beta$. The constant λ_4-lines in the figures are cut at some high values of λ_1, correspondingly to the assumed 10% precision on the κ's. This prevents the lines with large λ_4 values from reaching the SM line. Such an effect is generic and implies that an increased future precision will tend to eliminate the large (λ_1, λ_4) configurations that are compatible with $\mathrm{Br}(\mathcal{H} \to \gamma\gamma)^{(\mathrm{SM})}$. It should be noted, though, that the 'H^0-*scenario*' features smaller values of λ_1 than does the 'h^0-*scenario*' and would be thus somewhat simpler to interpret theoretically.

Of more interest are the small values of λ_1 that are compatible with $\mathrm{Br}(\mathcal{H} \to \gamma\gamma)^{(\mathrm{SM})}$. As stated previously these values correspond to zeroing the interference within the H^+, H^{++}

sector itself, that is when

$$\lambda_1 \simeq \lambda_1^0 \equiv -\frac{\lambda_4 m_{H^{++}}^2 Q_+^2 A_0^{\mathcal{H}}(m_{\mathcal{H}}^2/4m_{H^+}^2)}{2(m_{H^+}^2 Q_{++}^2 A_0^{\mathcal{H}}(m_{\mathcal{H}}^2/4m_{H^{++}}^2) + m_{H^{++}}^2 Q_+^2 A_0^{\mathcal{H}}(m_{\mathcal{H}}^2/4m_{H^+}^2))} \tag{3.17}$$

as can be easily seen from Eqs.(3.1, 3.6 - 3.9). Note that λ_1^0 has a non-trivial dependence on λ_4, μ, v_t through $m_{H^+}, m_{H^{++}}$. A somewhat striking behavior is found when λ_1 lies in the vicinity of λ_1^0; as illustrated numerically in Figs.2 (a), (b), an essentially unique value of λ_1^0 reproduces the SM diphoton branching ratio irrespective of λ_4. Clearly the $\lambda_4 = 0$ curve should cross the SM value when $\lambda_1 = 0$ since the couplings to H^+, H^{++} vanish in this case, Eqs.(3.6 - 3.9). In contrast, when $\lambda_4 \neq 0$, the low sensitivity to variations of λ_4 shown in the figures is far from obvious. A technical discussion of this point is relegated to appendix A. We insist here on the phenomenological consequences: in the previously discussed set of (λ_1, λ_4) with large values of λ_1 compatible with the SM prediction, a slight variation of λ_4 and thus of the H^+ and H^{++} masses would require a very different value of λ_1 to fine-tune to the SM value. When λ_1 is small we have the opposite situation, the SM compatible configuration becoming much more stable against the variation of H^+ and H^{++} masses through variations of λ_4. This corresponds to a domain with relatively light H^+ and H^{++} but still very difficult to exclude solely by the $\gamma\gamma$ (and $Z\gamma$) decay channels. Moreover this domain corresponding to small λ_1^0 does not require fine-tuning to retrieve the SM value. For instance one finds from Eq.(3.17) that $\lambda_1^0 \simeq -\lambda_4/6$ in the regime $\mu \ll v_t$ and $\lambda_1^0 \simeq -\lambda_4/10$, in the regime $\mu \gg v_t$ (see appendix A for further discussion).

The above features translate into two-fold domains in the $(\lambda_1, m_{H^{\pm\pm}})$ parameter space as illustrated in the upper plots of Fig.3 in terms of ratios of branching ratios,

$$R_{\gamma\gamma,Z\gamma}(\mathcal{H}) \equiv \frac{\mathrm{Br}_{\mathcal{H}\to\gamma\gamma,Z\gamma}^{\text{type II seesaw}}}{\mathrm{Br}_{\mathcal{H}\to\gamma\gamma,Z\gamma}^{\mathrm{SM}}} \approx \frac{(\Gamma_{\mathcal{H}\to gg} \times \mathrm{Br}_{\mathcal{H}\to\gamma\gamma,Z\gamma})^{\text{type II seesaw}}}{(\Gamma_{\mathcal{H}\to gg} \times \mathrm{Br}_{\mathcal{H}\to\gamma\gamma,Z\gamma})^{\mathrm{SM}}}. \tag{3.18}$$

The domain of large λ_1 is relevant for the lighter part of the $H^\pm, H^{\pm\pm}$ spectrum, while the small λ_1 domain is more substantial and extends to heavier charged scalar masses. The scans in Fig.3 are consistent with the U-BFB constraints as well as a loose lower bound of 110GeV on the $H^\pm, H^{\pm\pm}$ masses. Note that the latter bound does not conflict with [43], [44], as far as v_t is large enough so that the same-sign dilepton decay channels of $H^{\pm\pm}$ are not dominant (see also the discussion at the end of sec.V).

The $Z\gamma$ channel enjoys qualitatively the same properties as the ones discussed above; we note only some quantitative differences such as the absence of the large λ_1 SM-like solution

which lies well above the perturbative unitarity constraint as shown in Figs.2 (c),(d), which explains the absence of two distinct domains in Figs.3 (c), (d).

One also sees on Figs.2, 3 that changing the sign of λ_1 from positive to negative changes the interference effects from destructive to constructive. We discuss however more in detail the likeliness of $\lambda_1 < 0$ in the next section.

Finally it is interesting to understand the structure of the correlation between $\mathrm{Br}(\mathcal{H} \to \gamma\gamma)$ and $\mathrm{Br}(\mathcal{H} \to Z\gamma)$. We illustrate this correlation in Fig.4 for fixed values of μ and v_t and a scan over λ_1, λ_4 (and λ_2, λ_3 as well, the latter being however less relevant). The overall conical shape of the allowed domain traces the variation of λ_1, while the band results from the scan over λ_4. This behavior is generic: the two physical observables being of the form $|a + b\lambda_1|^2$, their parametric correlation through λ_1 will always be parabolic (rather than elliptic or hyperbolic). Thus, for fixed λ_4, the model predicts for each experimentally determined value of $R_{\gamma\gamma}$ two possible values of $R_{Z\gamma}$.[7] Present limits on $\mathcal{H} \to Z\gamma$ from ATLAS [45, 46] and CMS [47] are still very weak. Given the projections for future precisions on the measurement of the signal strength for this decay channel, putting them in the ballpark of 20% - 60% [24],[25], it is worth noting that typically an $R_{\gamma\gamma} \gtrsim 1$ will be consistent with the model either for $R_{Z\gamma} \gtrsim 1$ or for $R_{Z\gamma} \lesssim 0.2$. Thus the projected low precision on the $Z\gamma$ decay channel will nevertheless be sufficient to lift this degeneracy. However, as stesssed previously, should future data favor both $R_{\gamma\gamma}$ and $R_{Z\gamma}$ to be very close to the SM predictions, this by itself would neither constrain λ_4 to be close to zero nor the (doubly)- charged Higgs masses to be very heavy and lying in the decoupling limit.

IV. THEORETICAL CONSTRAINTS ON THE HIGGS SELF-COUPLINGS

In this section we would like to clarify the issue of the allowed regions in the $[\lambda_1, \lambda_4]$ parameter space when taking into account the full set of tree-level U-BFB constraints established in[15]. The virtual contributions of (doubly-)charged Higgses enhancing or suppressing the $\mathcal{H} \to \gamma\gamma$ decay channel branching ratio, first noted in [33] for $\lambda_1 > 0$, were reassessed in

[7] Note that the opposite is true too; for each $R_{Z\gamma}$ the model predicts two possible values of $R_{\gamma\gamma}$, since in fact the parabola is always tilted. This does not show on the plot because the tilt is extremely small, typically of order 1%, due to the smallness of $A_0^{\mathcal{H}}(\tau, M_Z^2/4m_i^2)$ as compared to $A_0^{\mathcal{H}}(\tau)$ entering respectively in $R_{Z\gamma}$ and $R_{\gamma\gamma}$. It follows that the second possible value for $R_{\gamma\gamma}$ is very large and totally irrelevant phenomenologically.

[16], [48] and [39] in the case $\lambda_1 < 0$ leading to stronger constraints on the model. Although we agree that $\lambda_1 < 0$ configurations are not strictly forbidden by the U-BFB constraints, these constraints have been only partially taken into account in the latter studies relying essentially only on two of the BFB constraints Eq.(B10). In fact the full set of U-BFB constraints strongly disfavors the $\lambda_1 < 0$ configurations. We provide hereafter and in appendix B a general proof of this property, but let us first give a numerical illustration: Fig.1 shows the ratio $R_{\gamma\gamma}$ as defined in Eq.(3.18) versus λ_1, for a chosen set of the remaining λ_i parameters. While $R_{\gamma\gamma}$ is indeed increased for $\lambda_1 < 0$, one clearly sees that the U-BFB constraints reduce drastically the allowed points which become increasingly scarce with increasingly negative λ_1. As was recognized in [16], to reach more negative λ_1 values one has to increase λ_2 and λ_3, see Eq.(B10). However, the point is that the scarcity of the allowed points will remain. More generally, the fully analytical form of the U-BFB constraints as given in [15] (see also Eqs.(B1 - B13)) allows an exact evaluation of the allowed hyper-volume in the four dimensional λ_i space. We state here the result, deferring the details of this somewhat tedious evaluation to appendix B: on the basis of a flat prior in the full λ_i space one finds that $\lambda_1 < 0$ accounts for $\sim 10\%$ of the allowed parameter space volume. Requiring $\lambda_1 < -0.5$ or $\lambda_1 < -1$ as considered in [16], [48], reduces the contribution to 3% for the former and down to $\sim 3‰$ for the latter. On the other edge, $\lambda_1 > 10$ accounts for $\sim 9\%$ while $\sim 80\%$ of the hyper-volume corresponds to $0 < \lambda_1 < 10$.[8]

Thus, in the absence of any underlying theoretical assumptions, based possibly on some UV completion of the model and favoring $\lambda_1 < 0$ or $\lambda_1 \gtrsim 10$, the above results should be taken at fair value. In particular the very strong constraint on the model inferred from $\mathcal{H} \to \gamma\gamma$ data in the regions $\lambda_1 < -1$ or $\lambda_1 < -0.5$, should be convoluted by the percent to per thousand probability of their occurrence! This comes for instance in contrast with the issue of taking values of the μ parameter much larger or much smaller than the electroweak scale, where in either case one can provide theoretical motivations, as discussed in section II.

[8] These figures are obtained for $\kappa = 8$ and can be somewhat sensitive to κ without changing though the overall conclusion as far as $\lambda_1 < 0$ is concerned. For instance taking $\kappa = 16$ reduces the probability of the latter to 7% while increasing tremendously that of $\lambda_1 > 10$ up to 40%. See table VI of appendix B.

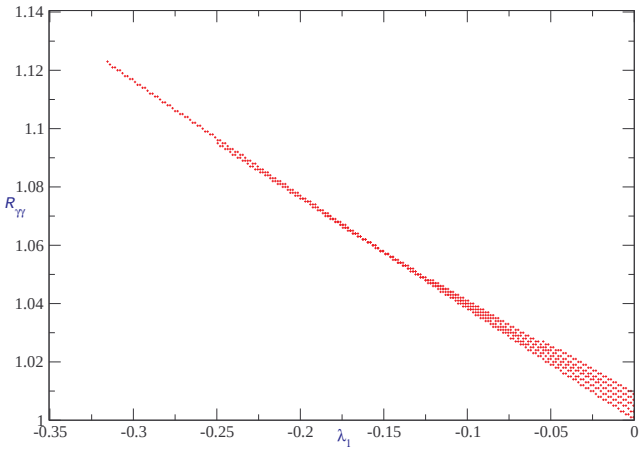

FIG. 1: Scatter plot for $R_{\gamma\gamma}$ versus λ_1 in the $\lambda_1 < 0$ plane with $\lambda = 0.52, \lambda_3 = 2, \lambda_2 = 0.2, v_t = 1$ GeV, $-10 \leq \lambda_4 \leq 2$ and $\mu = 1$GeV. One clearly sees that the U-BFB constraints reduce drastically the allowed λ_1 values which become increasingly scarce with increasingly negative λ_1.

V. INVISIBLE/UNDETECTED HIGGS DECAYS

In this section we examine the possible existence of non standard scalar states lighter than the observed ~ 125GeV SM-Higgs-like state. Such a configuration has attracted much attention in the recent literature on BSM physics, but has seldom been addressed in the context of the *type II seesaw* model. It corresponds to the H^0-*scenario* described in section II, where the heavier CP-even state H^0 becomes SM-like due to small values of the μ parameter, of order v_t or smaller. Such μ configurations should not be considered as marginal, even though they correspond to small parts of the parameter space. Possible model settings motivating these configurations have been briefly discussed in section II.

The would-be Majoron due to spontaneous violation of the lepton number induced by v_t [if μ were vanishing], receives then a small $\mathcal{O}(\mu)$ mass, Eq. (2.19), and is identified with the CP-odd physical state A^0. For such small μ the lighter CP-even state h^0 will have mainly a triplet component and is typically very light too, Eq.(2.17). The heavier CP-even state H^0 becomes essentially SM-like. Its mass can be made to match the observed value with arbitrary precision by fixing the parameter λ according to Eq. (2.23). In contrast, the charged and doubly charged states can be made (very) heavy by choosing sufficiently large (and negative) values of λ_4, Eqs. (2.20, 2.21). This freedom allows to match the present experimental lower bounds, in particular on the doubly-charged state mass, that is of order 410 GeV, [43, 44]. We will come back to this point at the end of the present section.

The dependence of the Higgs spectrum on the parameters of the model in the regime $\mu \lesssim v_t$ is given in Eqs.(2.17 - 2.21). Sufficiently small μ offers a rich phenomenology as the decay channels $H^0 \to h^0 h^{0(*)}, A^0 A^{0(*)}$ become kinematically favored with significant branching ratios. Indeed in the considered limit where H^0 carries essentially an $SU(2)_L$ doublet component, $|s_\alpha| \approx 1, c_\alpha \approx 0$, the $h^0 h^0 H^0$ and $A^0 A^0 H^0$ couplings become

$$g_{h^0 h^0 H^0} = g_{A^0 A^0 H^0} \simeq (\lambda_{14}^+) v_d + \mathcal{O}(v_t) \tag{5.1}$$

see Eqs.(2.33, 2.34), leading typically to electroweak scale enhanced Higgs into Higgs decays. The subsequent decays of h^0 and A^0 into fermions, gluons, or photons, will lead either to invisible or undetected H^0 decays that can be constrained by the global fit of the present ATLAS and CMS data to Higgs couplings [3], [4, 49] , or to four photon final states that are also constrained when interpreted in terms of two photon final states (collimated photons) [50]. Searches for invisible decay of the Higgs boson have been carried out by CMS and ATLAS from a variety of production processes. The two collaborations used the SM Higgs-strahlung $pp \to ZH$ cross section with SM Higgs boson at 125 GeV, and excluded an invisible branching ratio larger than 65% with 95% C.L. [51], [52]. The CMS collaboration has also performed a search for the invisible decay of the Higgs boson via the vector boson fusion process (VBF) and an upper limit of 69% with 95% C.L was set [53]. CMS did also a combination of Higgs-strahlung and VBF process analysis which improved slightly the upper limit on the Branching ratio of the invisible decay to 54% at the 95% C.L. [54]. These limits are still rather weak and will improve with future LHC runs.

On the other hand, global fit analyses performed on LHC data can in turn put limits on the invisible decay of the Higgs, [55–60]. The outcome of these studies depends of course on the allowed deviation of the coupling of the SM Higgs to SM particles. In a scenario where all couplings of the Higgs to SM particles are SM-like and the invisible decay of the Higgs allowed, the upper limit on the invisible branching ratio is 19% .

We show in Fig.9 contour plots of invisible/undetected decay branching ratios for a SM-like Higgs decaying into a pair of on-shell h^0 and A^0, in the $m_{h^0} \simeq m_{A^0}$ versus $|\lambda_{14}^+|$ plane, using the couplings given in Eq. (5.1). In the sequel we shall assume the nominal bound

$$|\lambda_{14}^+| \lesssim 0.05 \tag{5.2}$$

to cope with the present LHC upper limits on invisible/undetected SM Higgs decays in our scenario. Similar limits obtain if off-shell contributions are included, but would eventually

be weakened for much heavier h^0, A^0 that go beyond our scenario. We show in Fig. 5 the various H^0 branching ratios when varying the ratio $\frac{\mu}{v_t}$ or equivalently the $m_{h^0} \simeq m_{A^0}$ mass.

Moreover, due to their dominant triplet component, h^0 and A^0 are fermiophobic (except possibly for neutrinos), with couplings to up and down quarks and charged leptons suppressed by a factor $2v_t/v_d (\lesssim 8 \times 10^{-3})$ with respect to the SM Higgs and neutral Goldstone couplings. It follows that many of the exclusion limits on light ($\lesssim$ 10 GeV) CP-odd or CP-even Higgs states from radiative decays of J/ψ [61] or Υ [62, 63] do not apply, and obviously neither do the LHC limits from searches in the $\mu^+\mu^-$ decay channels [64, 65]. More importantly, some of the upper bounds set by LEP on the cross-sections for the processes $e^+e^- \to h^0A^0, h^0Z^0$, interpreted in the type II Two Higgs Doublet (2HDM(II))model and model-independently [66], [67], [68], or in the minimal supersymmetric SM [69], turn out to be partly relevant to the triplet-like h^0 and A^0 states as well. We note first that the $Z^0Z^0h^0$ coupling has a $4v_t/v_d$ suppression with respect to the SM $Z^0Z^0\mathcal{H}$ coupling, thus leading to a reduction of order 10^{-4} or less of the $e^+e^- \to h^0Z^0$ cross-section, two orders of magnitude smaller than the model-independent exclusion sensitivity at LEP for $e^+e^- \to h^0Z^0$ [66]. In contrast, the $Z^0h^0A^0$ derivative coupling in the *type II seesaw* is of the same magnitude as the SM $Z^0Z^0\mathcal{H}$ coupling. In fact the $Z^0h^0A^0$ coupling is, for most of the parameter space, given by $\frac{g}{c_w}$ as shown in Eqs. (2.29, 2.30), to be compared with the corresponding coupling in the case of the 2HDM(II), that is given by $c \times \frac{g}{2c_w}$ where c is a further mixing angle cosine suppression. Note the factor 2 difference between the two couplings. Following [66], the c^2 parameter in terms of which limits have been presented on the associated production of scalar/pseudo-scalar states with subsequent visible decays, can be re-expressed as the ratio of the cross-section $\sigma_{e^+e^-\to h^0A^0}$ to the SM cross-section $\sigma_{e^+e^-\to \mathcal{H}Z^0}$, up to a kinematic suppression factor; negative searches in the $e^+e^- \to h^0A^0$ channel have lead to exclusion domains in the m_{h^0}, m_{A^0} plane depending on the value of c^2 and the subsequent hadronic or leptonic decay rates of h^0 and A^0. The maximal value $c^2 = 1$ in the 2HDM(II) can in principle exclude large mass regions between 20 and 120GeV, [66]. To read off the exclusion domain for the *type II seesaw* model requires an extrapolation up to $c^2 = 4$, due to the factor 2 in the coupling noted above. Moreover, the LEP precision measurements of the Z-boson total width Γ_Z set stringent and complementary bounds on any extra contribution $\Delta\Gamma_Z$ from new decay channels, irrespective of the final states. From the quoted LEP value $\Gamma_Z = 2.4952 \pm 0.0023$GeV and the SM prediction $\Gamma_Z^{SM} = 2.4961 \pm 0.0010$GeV [70], one

can estimate the maximum allowed non-standard contribution to be $\Delta\Gamma_Z^{max} \simeq 4.2$MeV at the 95% C.L. As we will see, the combination of the above constraints leads to particularly strong upper bounds either on v_t or on $v_t \times (\lambda_{14}^+)/\lambda$ if $m_{A^0} \simeq m_{h^0} \lesssim 80$GeV.

In Fig.6 we show the mass region in the (m_{h^0}, m_{A^0}) parameter space compatible with the constraint $\Gamma(Z \to h^0 A^0) \leq \Delta\Gamma_Z^{max}$ where we used the $Z^0 h^0 A^0$ tree-level coupling. Specifying to the *type II seesaw*, h^0 and A^0 are essentially degenerate in mass, c.f. Eq.(2.22). The above bound translates then into the irreducible lower bound

$$m_{h^0} \simeq m_{A^0} \gtrsim 44.3\text{GeV} \tag{5.3}$$

or equivalenty, in terms of the model parameters into $\mu \gtrsim 4.6 \times 10^{-2}\ v_t$. On the other hand, if h^0 and A^0 decay 100% into a $b\bar{b}$ pair, then the most stringent limit from $e^+e^- \to h^0 A^0$ at LEP2 C.M. energies $\sqrt{s} = 183, 187$GeV given by [66] for $c^2 \simeq 1$ will exclude the mass range $33\text{GeV} \lesssim m_{h^0} (\simeq m_{A^0}) \lesssim 78\text{GeV}$. In our case h^0 and A^0 decay predominantly either into $b\bar{b}$ for sufficiently large values of v_t, or invisibly into $\nu\nu + \bar{\nu}\bar{\nu}$ for much smaller values of v_t, see Fig. 7. However, in the region dominated by the $b\bar{b}$ channel, the corresponding branching ratio quickly reaches, but does not exceed, $\sim 80 - 85\%$. Furthermore, as can be seen from Figs. 11, 12, the next-to-dominant decay channel is $\tau^+\tau^- \lesssim 9\%$, except for some parts of the parameter space where it can be dominated by $\gamma\gamma$ decays of h^0 , Fig. 12(b). [In evaluating the branching ratios we have taken into account the leading perturbative QCD corrections to the CP-even and CP-odd Higgs decays into hadronic two-body final states; see later discussion and appendix C for more details.] Given these typical branching ratios, one can not read off directly the limits from the published results (see, e.g. [66], [71] and references therein) where a 100% branching ratio into $b\bar{b}$ or into $\tau^+\tau^-$ was assumed for the decaying (pseudo)scalars, and in some cases SM-like Higgs branching ratios. In our case, a complete study would require a statistical combination of the various decay channels, re-using LEP data. Since we are merely interested here in how to evade these constraints in a conservative way, we adopt the simplifying assumption of associating the total decay width of either h^0, A^0 into visible final states, $b\bar{b}, \tau^+\tau^-, gg, q\bar{q}, \gamma\gamma, ...$, exclusively with $b\bar{b}$ final state. This assumption leads to conservative limits from the LEP analyses since bounds from 100% branching ratio into $b\bar{b}$ are stronger than combined bounds when a small fraction of decay into other final states is allowed. Thus, hereafter we will denote by $Br(A^0, h^0 \to b\bar{b})$ the *total visible* decay branching ratios of the two light states. Furthermore, A^0 and h^0 having a very

small doublet component can feature substantial branching ratios into $\nu\nu + \bar{\nu}\bar{\nu}$ final state depending on the magnitude of the neutrino Yukawa couplings $Y_{\nu i}$ for the three neutrino flavors, Eq. (2.6). The corresponding decay width will scale like $\sum_{i=1}^{3} m_{\nu_i}^2/v_t^2$, to be contrasted with that of visible decays which scale like v_t^2 and $v_t^2 \times (\lambda_{14}^+)^2/\lambda^2$ respectively for A^0 and h^0, see table II.[9] Since we associate all visible final states with $b(\bar{b})$, the relevant quantities are

$$\begin{aligned} b^2 &\equiv Br(A^0 \to b\bar{b}) \times Br(h^0 \to b\bar{b}) \\ (b\nu)^2 &\equiv Br(A^0 \to b\bar{b}) \times Br(h^0 \to \nu\nu + \bar{\nu}\bar{\nu}) + Br(A^0 \to \nu\nu + \bar{\nu}\bar{\nu}) \times Br(h^0 \to b\bar{b}) \quad (5.4) \\ (\nu\nu)^2 &\equiv Br(A^0 \to \nu\nu + \bar{\nu}\bar{\nu}) \times Br(h^0 \to \nu\nu + \bar{\nu}\bar{\nu}) \end{aligned}$$

with $b^2 + (b\nu)^2 + (\nu\nu)^2 = 1$. It follows that we can re-interpret the quantity b^2 as a modification of the scaling factor c^2 used in the LEP analyses, since $b^2 < 1$ signals a reduction of the expected total number of *detectable* signal events. This is so because either the two higgses decayed invisibly into neutrinos, when $(\nu\nu)^2$ is substantial, or, when $(b\nu)^2$ is substantial, the SM Higgs LEP searches through the $b\bar{b} + E_{\rm miss}$ final state cannot be re-interpreted as constraints on our model, apart from possibly a region around $m_{A^0} \simeq m_{h^0} \simeq 90$GeV since the latter searches triggered on missing energy close to m_Z, see e.g. [72]. More specifically, taking into account the factor 2 enhancement in the $Z^0 h^0 A^0$ coupling noted earlier, the proper identification is $c^2 \equiv 4b^2$ and one can now use directly the exclusion domains given in fig.13 (b) of ref. [66] up to $c^2 = 1$. We reproduce in table IV an excerpt of these domains in the mass configuration $m_{A^0} \simeq m_{h^0}$ relevant for our model. Since in our case c^2 can take values up to 4, we need to extrapolate these exclusion domains. While theoretically the cross-section $\sigma_{e^+e^- \to h^0 A^0}$ scales linearly with c^2, from which bounds on $m(\equiv m_{h^0} \simeq m_{A^0})$ can be easily extracted using Eq. (D2), one should keep in mind that the experimental bounds on c^2 depend on detection efficiencies of $h^0 A^0$ events and thus on m itself. We have indeed checked that the set of upper (lower) mass bounds in table IV do not fit to a straight line in the $[c^2, \sigma_{e^+e^- \to h^0 A^0}]$ plane. However, we find that the subset of the upper part of the

[9] We will consider for the numerical illustrations the two extreme values $(\sum_{i=1}^3 m_{\nu_i}^2)|_{min} = 2.48 \times 10^{-21}\text{GeV}^2$ and $(\sum_{i=1}^3 m_{\nu_i}^2)|_{max} = 1.78 \times 10^{-20}\text{GeV}^2$, compatible with neutrino oscillation limits $|m_{\nu_2}^2 - m_{\nu_1}^2| \simeq 7.6 \times 10^{-23}\text{GeV}^2$, $|m_{\nu_3}^2 - m_{\nu_1}^2| \simeq 2.4 \times 10^{-21}\text{GeV}^2$ and the cosmological mass bound $\sum_{i=1}^3 m_{\nu_i} < 0.23 \times 10^{-9}$GeV. Note that the minimum value requires normal mass hierarchy and the maximum value inverted mass hierarchy. For later discussions, we refer to these two extreme cases respectively as normal minimal (NMIN) and inverted maximal (IMAX).

sample points corresponding to $c^2 = 0.3, 0.5, 1$ lies on a straight line within 1%. We take this as signaling a high detection efficiency in this part of the parameter space and rely on this linear fit to extrapolate to higher values of c^2 as given in table V.

c^2	< 0.1	< 0.12	< 0.15	< 0.3	< 0.5	< 1
LEP-excluded $m_{h^0} \simeq m_{A^0}$(GeV)	$[49.9, 56.8]$	$[40.3, 63.7]$	$[38.3, 67.4]$	$[35.9, 70.9]$	$[34.8, 75]$	$[33.0, 78.1]$

TABLE IV: approximate intervals of mass exclusion, extracted from Fig.13 (b) of the OPAL analysis [66].

c^2	< 2	< 3	< 4
$m_{h^0} \simeq m_{A^0}$(GeV)	$[32.3, 79.8]$	$[32.1, 80.4]$	$[31.9, 80.7]$

TABLE V: Mass exclusion intervals extrapolated from Fig.13 (b) of [66]; see text for more details.

Note that apart from $c^2 \lesssim 0.1$, the lower edges of the excluded intervals given in the tables are lower than the irreducible lower bound of Eq. (5.3). The allowed regions are thus determined solely by the upper edges of these intervals that correspond to lower mass bounds. As noted earlier, these bounds are controlled by the relative magnitudes of the branching ratios $b^2(= c^2/4), (b\nu)^2, (\nu\nu)^2$ defined in Eq. (5.4) that depend on v_t and λ_{14}^+. However, the visible decay widths of A^0 and h^0 will also be of an issue, as the bounds would be invalidated if at least one of the two particles decays outside the detector. The decay length $c\tau$ of an A^0 decaying mainly into $b\bar{b}$, reads, in the instantaneous decay approximation and at tree-level,

$$c\tau_{A^0} \simeq 3.44 \times 10^{-8} \times \frac{(s - 4\, m_{A^0}^2)^{\frac{1}{2}}}{m_{A^0}^2\, v_t^2} \text{ [meters]} \tag{5.5}$$

in a reference frame where the A^0 energy is $E_{A^0} = \sqrt{s}/2$ [GeV], (see also appendix D). Similarly, one finds for h^0

$$c\tau_{h^0} \simeq 0.94 \times 10^{-8} \times \frac{(s - 4\, m_{h^0}^2)^{\frac{1}{2}}}{m_{h^0}^2\, v_t^2 (\lambda_1 + \lambda_4)^2} \text{ [meters]} \tag{5.6}$$

where we took into account the enhancing factor $(\lambda_{14}^+)^2/\lambda^2$ in the width, with $\lambda \simeq 0.52$ as dictated by the SM-like Higgs mass. We show in Fig.8 the $c\tau_{A^0}$ contours in the (m_{A^0}, v_t) plane assuming A^0 produced through $e^+e^- \to h^0A^0$ at the LEP2 C.M. energy $\sqrt{s} = 183$GeV and a visible decay mainly into $b\bar{b}$ pairs. It is instructive to assess the effect of the QCD corrections to $\Gamma(A^0 \to b\bar{b})$ which we included in Fig.8 (right), as compared to the naive tree-level width Fig.8 (left) given by Eq. (5.5), see also appendix C. In the mass parameter space under consideration a fiducial 3-meter decay length is reached for v_t in the range $\sim (1.8-4) \times 10^{-5}$GeV; but for such small values of v_t the branching ratios b^2 and $(b\nu)^2$ are already largely overwhelmed by the totally invisible decay branching ratio $(\nu\nu)^2$ irrespective of the allowed values of λ_{14}^+. It follows that the A^0 decay length does not play a role here. In contrast, the extra dependence on λ_{14}^+ in $c\tau_{h^0}$ will bring v_t back in ranges where b^2 and $(b\nu)^2$ are dominant, as we shall discuss below. Furthermore, we find that $(b\nu)^2$ is dominated by $Br(A^0 \to b\bar{b}) \times Br(h^0 \to \nu\nu + \bar{\nu}\bar{\nu})$ for $\lambda_{14}^+ \lesssim 0.55$, which is always satisfied due to Eq. (5.2). Thus a large $c\tau_{h^0}$ will not add new constraints when $(b\nu)^2$ dominates over b^2, since an h^0 not decaying in the detector or decaying into neutrinos lead to the same experimental (missing energy) signature. For a better understanding of the interplay between the various constraints it is worth noting that due to the huge hierarchy between the neutrino mass scale and the electroweak scale, the relative magnitudes of the various branching ratios will involve large/small numbers in the (v_t, λ_{14}^+) plane. For instance, taking $m_{h^0} \simeq m_{A^0} = 80$GeV and $\sum m_\nu^2|_{min}$ (see footnote 9) one finds the following necessary and sufficient conditions:

(I) b^2 dominates $(b\nu)^2$ when $v_t \gtrsim 4 \times 10^{-4}$GeV and $(\lambda_{14}^+)^2 \gtrsim (-3.13 + 1.21 \times 10^{14} \times (v_t[\text{GeV}])^4)^{-1}$

(II) b^2 dominates $(\nu\nu)^2$ when $|\lambda_{14}^+| \gtrsim 1.46 \times 10^{-14} \times (v_t[\text{GeV}])^{-4}$

(III) $(\nu\nu)^2$ dominates $(b\nu)^2$ when $v_t \lesssim 4 \times 10^{-4}$GeV and $(\lambda_{14}^+)^2 \lesssim -0.32 + 8.23 \times 10^{-15} \times (v_t[\text{GeV}])^{-4}$

Although the figures will depend on the neutrino mass assumptions as well as the h^0, A^0 mass, we find that this dependence remains moderate allowing to draw generic conclusions by examining the relative magnitudes of the bounds appearing in (I), (II) and (III):
-if (I) is satisfied then (II) is satisfied as well but (III) violated, leading to the hierarchy $b^2 > (b\nu)^2 > (\nu\nu)^2$. However, taking into account the LHC inferred bound Eq. (5.2) one finds from

(I) that a window where b^2 starts dominating opens only when $v_t \gtrsim 1.3 \times 10^{-3}$GeV; in the domain 4×10^{-4}GeV$\lesssim v_t \lesssim 1.3 \times 10^{-3}$GeV the $(b\nu)^2$ branching ratio will dominate, starting from $(b\nu)^2 \approx 50\% \approx (\nu\nu)^2 \gg b^2$ near the lower edge of the domain for any $\lambda_{14}^+ \lesssim 0.05$, a reversed hierarchy $(b\nu)^2 \gtrsim b^2 \gg (\nu\nu)^2$ obtains near the upper edge. For smaller $\lambda_{14}^+ (\lesssim 0.01)$, $(b\nu)^2$ is above 90-95% for most of the upper part of the domain.

-if $v_t \gtrsim 1.3 \times 10^{-3}$GeV, condition (I) applies fully and b^2 quickly reaches 99% for increasing v_t and $\lambda_{14}^+ \lesssim 0.05$. For smaller values of λ_{14}^+ as would be implied by improved future LHC limits on invisible/undetected SM-Higgs decays, $(b\nu)^2$ becomes substantial again and also an increased $c\tau_{h^0}$ will eventually contribute to weaken the LEP constraints on scalar and pseudo-scalar states as discussed previously. Since this is the region where the LEP2 constraints can be the most stringent, we illustrate in Fig.10 the rather busy configuration of the interplay among b^2, $(b\nu)^2$ and $c\tau_{h^0}$. Fig.10(a) shows the $c\tau_{h^0} = 3$meters lines for various h^0 masses, below which h^0 is long-lived and the LEP2 limits from jets and/or lepton decays do not apply. One can read from figures 10(b), (c), corresponding respectively to the NMIN and IMAX neutrino mass configurations, the relative contributions of the $bb\bar{b}\bar{b}$ final state as compared to the $b\bar{b}, \nu\nu + \bar{\nu}\bar{\nu}$ final state and the effect of the h^0 decay length, in the v_t, λ_{14}^+ parameter space. Although smaller neutrino masses lead to larger visible decay branching ratios and thus in principle to stronger exclusion limits in a given part of the parameter space, the h^0 decay length reduces this effect, as can be seen by comparing figures (b) and (c). For instance, in the NMIN configuration $m_{h^0} \simeq 55$GeV would not be excluded by LEP even for $b^2 \approx 98.75\%$ (corresponding to $c^2 \simeq 3.95$, see figure (b) and table V) unless $\lambda_{14}^+ \gtrsim 3.4 \times 10^{-4}$. Exclusion for smaller c^2 would require larger λ_{14}^+; e.g. $c^2 = 3.5$ would exclude $m_{h^0} \simeq 55$GeV from LEP negative searches only if $\lambda_{14}^+ \gtrsim 1.3 \times 10^{-3}$ and $v_t \gtrsim 1.4 \times 10^{-2}$GeV, whereas $c^2 = 1$ would do so for $\lambda_{14}^+ \gtrsim 5.8 \times 10^{-3}$ and $v_t \gtrsim 3 \times 10^{-3}$GeV. Increasing m_{h^0} reduces the decay length and thus the v_t, λ_{14}^+ bounds above which the LEP exclusions hold. For example the exclusion of $m_{h^0} \simeq 75$GeV for $c^2 = 1$, c.f. table IV, applies only if $\lambda_{14}^+ \gtrsim 2.4 \times 10^{-3}$, $v_t \gtrsim 4.7 \times 10^{-3}$GeV. Comparing the two latter examples illustrates the existence of windows in the (v_t, λ_{14}^+) parameter space where heavier masses are excluded and lighter ones still allowed (!), in contrast with the model-independent LEP exclusion domains [66]. One should however keep in mind that whenever b^2 is reduced in favor of $(b\nu)^2$ or becomes ineffective due to large h^0decay length, the same experimental signature of two b-jets and missing energy ensues. The SM-Higgs search through the $e^+e^- \to ZH^0 \to \nu\bar{\nu}b\bar{b}$

channel at LEP can then in principle be reinterpreted to exclude $A^0(h^0)$ masses of order m_Z. (Conservatively one could assume an exclusion of the domain $(76, 120)$GeV whenever $(b\nu)^2$ becomes substantial, even though a dedicated study would be necessary to take properly into account the corresponding backgrounds and rates, see [72].)

In the IMAX neutrino mass configuration, the LEP exclusions apply for smaller parts of the parameter space as the branching ratio into visible decays is smaller. The effect of the decay length is however less important since the c^2 contour lines are pushed upwards, cf. Fig.10(c). For instance λ_{14}^+ has now to be smaller than 1.4×10^{-4} for the $c^2 \simeq 3.95$ line to become ineffective regarding the LEP exclusions. All in all, we do not expect the re-interpretation of the LEP analyses to depend too much on the neutrino mass assumptions. It should be noted, though, that the very large hierarchy between the neutrino and electroweak scales implies a large sensitivity to v_t, λ_{14}^+ in the vicinity of $b^2 \simeq 100\%$: the corresponding $c^2 = 4$ line lies way out of the plots in Fig.10(b),(c) and does not intersect anymore the fiducial $c\tau_{h^0} = 3$ line. This again illustrates the fact that a smaller branching ratio for visible decays does not only imply smaller exclusion mass bounds for h^0, A^0 but also allows for unexcluded domains even below these bounds.

-when (III) is satisfied b^2 becomes negligible compared to $(\nu\nu)^2$ and $(b\nu)^2$; the latter reaching at best 50%, could be used for partial exclusion as discussed above. *Finally, when $v_t \lesssim 10^{-4}$GeV, the invisible decay branching ratio $(\nu\nu)^2$ reaches 98-99% even for the loose bound $\lambda_{14}^+ \lesssim 1$, thus evading all LEP constraints on scalar and pseudo-scalar states.* This conclusion holds irrespective of the size of λ_{14}^+, that is even if further reduced by future LHC limits on invisible/undetected decays of the (SM-like) Higgs. It is noteworthy that the tininess of v_t, required to account for (Majorana) neutrino masses in a natural setting of the model with Y_ν of order one, automatically invalidates the LEP bounds on light scalars.

We close this section with some comments on the (doubly-)charged states in the H^0-*scenario*. As stated previously the present experimental bounds on $m_{H^{++}}$ are in excess of 410 GeV or so and will be improved in the next LHC run. These bounds are obtained under the assumption of same-sign di-lepton decays with branching ratio one [43, 44], and can thus be much weaker (~ 90 GeV) if the $W^+W^{+(*)}$ and/or $W^+H^{+(*)}$ decay channels of H^{++} become important [73–75]. One should, however, keep in mind that this weakening requires increasingly large values of v_t that might become hardly consistent with the H^0-

scenario whose viability implies typically very small values of this parameter, as we have shown in this section. For $v_t \lesssim 10^{-4}$ GeV where the LEP constraints are totally evaded, the present and future bounds from same-sign di-lepton searches at the LHC fully apply, since $Br(H^{++} \to l^+l^+) \sim 1$ in this case. In the domain 4×10^{-4} GeV$\lesssim v_t \lesssim 1.3 \times 10^{-3}$ GeV for which the LEP exclusion domains are significantly reduced, except for a small region around the Z-boson mass, one finds $0.54 \lesssim Br(H^{++} \to W^+W^{+(*)}) \lesssim .99$ for $m_{H^{++}} \sim 400$GeV, signaling a reduction of the present LHC bounds to roughly $m_{H^{++}} \gtrsim 160$ GeV. Note also that the decay channel $H^{++} \to W^+H^{+*}$ plays no role in the H^0-*scenario* due to the small mass splitting between the H^+ and H^{++} states, Eqs. (2.20, 2.21).

VI. CONCLUSION

There are mainly two dynamical regimes leading to electroweak scale states in the scalar sector of the *type II seesaw* model. In this paper we examined various phenomenological features of these regimes and highlighted in particular the viability of the H^0-*scenario* where two electrically neutral CP-even and CP-odd scalar states are lighter than the discovered 125 GeV Higgs-like state, and still compatible with LEP and present LHC constraints. The SM properties of the Higgs-like state are naturally accounted for due to the large hierarchy between the neutrino and the electroweak mass scales. Thus, future confirmation of the SM properties of the 125 GeV state with improved precision would not invalidate this scenario. Even more, the diphoton and $Z\gamma$ decay channels can also remain very close to their SM values due to a somewhat generic screening of the effects of electroweak scale charged states. Stringent lower bounds from future direct searches on the masses of the latter states, combined with strict exclusion limits on invisible decays of the 125 GeV state, will be eventually needed to disfavor this H^0-*scenario*.

Appendix A: effective fixed point in $\mathcal{H} \to \gamma\gamma, Z\gamma$.

In section III C we noted numerically a peculiar behavior of $\mathcal{H} \to \gamma\gamma, Z\gamma$ in the vicinity of the SM value. We give here a more detailed quantitative study in the case of $\mathcal{H} \to \gamma\gamma$, showing that this behavior is a direct consequence of the analytical structure of the (doubly-)charged Higgs virtual contributions to the amplitude,

$$\mathcal{A} \equiv Q_+^2 \tilde{g}_{\mathcal{H}H^+H^-} A_0^{\mathcal{H}}(\tau_{H^+}) + Q_{++}^2 \tilde{g}_{\mathcal{H}H^{++}H^{--}} A_0^{\mathcal{H}}(\tau_{H^{++}}) \tag{A1}$$

entering Eq.(3.1), together with the form of their masses

$$m_{H^\pm}^2 = \frac{(v_d^2 + 2v_t^2)[2\sqrt{2}\mu - \lambda_4 v_t]}{4v_t} \tag{A2}$$

$$m_{H^{\pm\pm}}^2 = \frac{\sqrt{2}\mu v_d^2 - \lambda_4 v_d^2 v_t - 2\lambda_3 v_t^3}{2v_t} \tag{A3}$$

(see e.g. [33]).

Treating $\mathcal{A}$ as a function of λ_1, λ_4, the observed effective fixed point in Figs.2 (a), (b) can be understand as meaning that for $\lambda_1 = \lambda_1^0$ as defined in Eq. (3.17), the gradient $\vec{\nabla}\mathcal{A}$ in the λ_1, λ_4 space is essentially orthogonal to the displacement vector $d\vec{\lambda} \equiv (d\lambda_1, d\lambda_4)$ in the directions satisfying $|d\lambda_1| \ll |d\lambda_4|$. This approximate orthogonality occurs if $\partial\mathcal{A}/\partial\lambda_4 \ll \partial\mathcal{A}/\partial\lambda_1$, in which case one has $d\mathcal{A} = \vec{\nabla}\mathcal{A}.d\vec{\lambda} \simeq 0$ near the point $\mathcal{A}_{\lambda_1=\lambda_1^0} = 0$, thus leading to the observed very weak sensitivity to λ_4 when $\mathcal{H} \to \gamma\gamma$ coincides with the SM value. Taking into account Eqs. (3.4, 3.5, A2, A3) and the present phenomenological bounds on $m_{H^+}, m_{H^{++}}$ that imply the occurrence of arcsin functions in Eqs. (A1, 3.17), a somewhat lengthy but straightforward calculation leads to the following expressions for $\frac{\partial\mathcal{A}/\partial\lambda_4}{\partial\mathcal{A}/\partial\lambda_1}|_{\lambda_1=\lambda_1^0}$ in two relevant regimes.

1) $\frac{v_t}{v_d} \ll 1$:

$$\begin{aligned} \frac{\partial\mathcal{A}/\partial\lambda_4}{\partial\mathcal{A}/\partial\lambda_1}|_{\lambda_1=\lambda_1^0} &= \frac{Q_+^2}{2(Q_+^2+Q_{++}^2)} - \frac{\lambda_4 Q_+^2 Q_{++}^2}{2\sqrt{2}(Q_+^2+Q_{++}^2)^2}\frac{v_t}{\mu} + \mathcal{O}((\frac{v_t}{v_d})^{\frac{3}{2}}) \\ &\simeq \frac{1}{10} - 5.6\times 10^{-2}\lambda_4\frac{v_t}{\mu} + \mathcal{O}((\frac{v_t}{v_d})^{\frac{3}{2}}) \end{aligned} \tag{A4}$$

with

$$\begin{aligned} \lambda_1^0 &= -\frac{\lambda_4 Q_+^2}{2(Q_+^2+Q_{++}^2)} + \frac{\lambda_4^2 Q_+^2 Q_{++}^2}{4\sqrt{2}(Q_+^2+Q_{++}^2)^2}\frac{v_t}{\mu} + \mathcal{O}((\frac{v_t}{v_d})^{\frac{3}{2}}) \\ &\simeq -\frac{\lambda_4}{10} + 0.14\times\lambda_4^2\frac{v_t}{\mu} + \mathcal{O}((\frac{v_t}{v_d})^{\frac{3}{2}}) \end{aligned} \tag{A5}$$

These expansions are valid for $\lambda_4 \frac{v_t}{\mu} \simeq \mathcal{O}(1)$ or $\gg \mathcal{O}(1)$.

2) $\frac{\mu}{v_t} \ll 1$, $\frac{v_t}{v_d} \ll 1$ and large λ_4:

$$\begin{aligned}
\frac{\partial\mathcal{A}/\partial\lambda_4}{\partial\mathcal{A}/\partial\lambda_1}|_{\lambda_1=\lambda_1^0} &= \frac{Q_+^2}{2Q_+^2+Q_{++}^2} + \frac{16\sqrt{2}}{15}\frac{Q_+^2Q_{++}^2(Q_+^2+Q_{++}^2)}{(2Q_+^2+Q_{++}^2)^3\lambda_4^2}\frac{m_{\mathcal{H}}^2}{v_d^2}\frac{\mu}{v_t} \\
&\quad -\frac{Q_+^2Q_{++}^2(362Q_+^2+293Q_{++}^2)}{1575(2Q_+^2+Q_{++}^2)^3\lambda_4^2}\frac{m_{\mathcal{H}}^4}{v_d^4} + \mathcal{O}(\frac{\mu^2}{v_t^2},\frac{v_t^2}{v_d^2},\lambda_4^{-\frac{5}{2}}) \\
&\simeq \frac{1}{6} + (3.6\times10^{-2}\frac{\mu}{v_t} - 1.2\times10^{-3})\frac{1}{\lambda_4^2} + \mathcal{O}(\frac{\mu^2}{v_t^2},\frac{v_t^2}{v_d^2},\lambda_4^{-\frac{5}{2}}) \qquad \text{(A6)}
\end{aligned}$$

with

$$\begin{aligned}
\lambda_1^0 &= -\frac{\lambda_4 Q_+^2}{2Q_+^2+Q_{++}^2} + \frac{\sqrt{2}Q_+^2Q_{++}^2}{(2Q_+^2+Q_{++}^2)^2}(\frac{16}{15}\frac{(Q_+^2+Q_{++}^2)}{(2Q_+^2+Q_{++}^2)\lambda_4}\frac{m_{\mathcal{H}}^2}{v_d^2} - 1)\frac{\mu}{v_t} \\
&\quad + \frac{4}{15}\frac{Q_+^2Q_{++}^2}{(2Q_+^2+Q_{++}^2)^2}\frac{m_{\mathcal{H}}^2}{v_d^2} - \frac{Q_+^2Q_{++}^2(362Q_+^2+293Q_{++}^2)}{1575(2Q_+^2+Q_{++}^2)^3\lambda_4}\frac{m_{\mathcal{H}}^4}{v_d^4} + \mathcal{O}(\frac{\mu^2}{v_t^2},\frac{v_t^2}{v_d^2},\lambda_4^{-\frac{3}{2}}) \\
&\simeq -\frac{\lambda_4}{6} + (-0.16 + \frac{3.6\times10^{-2}}{\lambda_4})\frac{\mu}{v_t} + 7.6\times10^{-3} - \frac{1.2\times10^{-3}}{\lambda_4} + \mathcal{O}(\frac{\mu^2}{v_t^2},\frac{v_t^2}{v_d^2},\lambda_4^{-\frac{3}{2}}) \qquad \text{(A7)}
\end{aligned}$$

Equations (A4, A6) illustrate the conditions under which the effective fixed point behavior is reached. In particular in the regime of large μ, this behavior is expected to be somewhat stronger than in the regime $\mu \ll v_t$.

Appendix B: $\lambda_1 < 0$ versus $\lambda_1 > 0$ hyper-volumes

We provide here the detailed evaluation of the result stated in section IV. We first recall the full set of U-BFB analytical constraints (see [33] for more details), recasting them here in separate sectors for the couplings:

$\lambda, \lambda_2, \lambda_3$ *sector:*

$$0 \leq \lambda \leq \frac{2}{3}\kappa\pi \qquad \text{(B1)}$$

$$\lambda_2 + \lambda_3 \geq 0 \;\;\&\;\; \lambda_2 + \frac{\lambda_3}{2} \geq 0 \qquad \text{(B2)}$$

$$\lambda_2 + 2\lambda_3 \leq \frac{\kappa}{2}\pi \qquad \text{(B3)}$$

$$4\lambda_2 + 3\lambda_3 \leq \frac{\kappa}{2}\pi \qquad \text{(B4)}$$

$$2\lambda_2 - \lambda_3 \leq \kappa\pi \qquad \text{(B5)}$$

λ_1, λ_4 *sector:*

$$|\lambda_1 + \lambda_4| \leq \kappa\pi \tag{B6}$$

$$|\lambda_1| \leq \kappa\pi \tag{B7}$$

$$|2\lambda_1 + 3\lambda_4| \leq 2\kappa\pi \tag{B8}$$

$$|2\lambda_1 - \lambda_4| \leq 2\kappa\pi \tag{B9}$$

mixed sector:

$$\lambda_1 + \sqrt{\lambda(\lambda_2 + \lambda_3)} \geq 0 \;\; \& \;\; \lambda_1 + \sqrt{\lambda(\lambda_2 + \frac{\lambda_3}{2})} \geq 0 \tag{B10}$$

$$\lambda_1 + \lambda_4 + \sqrt{\lambda(\lambda_2 + \lambda_3)} \geq 0 \;\; \& \;\; \lambda_1 + \lambda_4 + \sqrt{\lambda(\lambda_2 + \frac{\lambda_3}{2})} \geq 0 \tag{B11}$$

$$|\lambda_4| \leq \min\{M_+, M_-\} \tag{B12}$$

$$|2\lambda_1 + \lambda_4| \leq \sqrt{2(\lambda - \frac{2}{3}\kappa\pi)(4\lambda_2 + 3\lambda_3 - \frac{\kappa}{2}\pi)} \tag{B13}$$

where

$$M_\pm \equiv \sqrt{(\lambda \pm 2\kappa\pi)(\lambda_2 + 2\lambda_3 \pm \frac{\kappa}{2}\pi)} \tag{B14}$$

The correspondence with the equations of ref.[15] is as follows:
(B1) – (B5) $\leftrightarrow$ (6.14) – (6.18); (B6) – (B8) $\leftrightarrow$ (6.4) – (6.6); (B10) $\leftrightarrow$ (6.2); (B11) $\leftrightarrow$ (6.3); (B12)$\leftrightarrow$ (6.19); (B13)$\leftrightarrow$ (6.20) and (B9) $\leftrightarrow$ (6.12). [Note that (6.12) was missing in the summary but included in the calculations in [15].]

The domain delimited by the above equations is defined by intersections of hyperplanes and hyperbolas, thus in principle completely manageable analytically. The two-fold ambiguity in determining the minimum in Eq.(B12) can be easily lifted by noting that

$$\lambda + 4(\lambda_2 + 2\lambda_3) < 0 \Leftrightarrow \; \min\{M_+, M_-\} = M_+$$
$$\lambda + 4(\lambda_2 + 2\lambda_3) > 0 \Leftrightarrow \; \min\{M_+, M_-\} = M_-$$

Thus one just needs to add the simple hyperplane

$$\lambda + 4(\lambda_2 + 2\lambda_3) = 0 \tag{B15}$$

to the set of boundary equations (B1 - B13).

Moreover, to simplify the subsequent discussion without loss of generality, we will take hereafter $\lambda = \dfrac{\pi}{6}$ which corresponds to $m_{\mathcal{H}} \simeq 126\text{GeV}$ with $v_t/v_d \ll 1$.

The aim is to compare the relative sizes of the two hyper-volumes $V_\pm$

$$V_\pm \equiv \int_{\mathcal{D}_\pm} \mathrm{d}\lambda_2 \, \mathrm{d}\lambda_3 \, \mathrm{d}\lambda_4 \, \mathrm{d}\lambda_1 \tag{B16}$$

where $\mathcal{D}_+, \mathcal{D}_-$ denote the sub-domains defined by Eqs.(B1 - B13) and respectively $\lambda_1 > 0$ and $\lambda_1 < 0$. Equations (B2 - B5) can be worked out explicitly leading to piecewise integrals over λ_2, λ_3. Taking into account Eq.(B15), one can finally write V_+ in the form:

$$\begin{aligned}
V_+ \;=\; & \int_0^{\frac{3\kappa\pi}{10}} \mathrm{d}\lambda_3 \int_{-\frac{\lambda_3}{2}}^{\frac{\kappa\pi}{8}-\frac{3\lambda_3}{4}} \mathrm{d}\lambda_2 \int_0^{\kappa\pi} \mathrm{d}\lambda_1 \int_{-M_-}^{M_-} \mathrm{d}\lambda_4 \, \mathcal{B}[\lambda_1,\lambda_2,\lambda_3,\lambda_4] \\
& + \int_{\frac{3\kappa\pi}{10}}^{\frac{\kappa\pi}{3}} \mathrm{d}\lambda_3 \int_{-\frac{\lambda_3}{2}}^{\frac{\kappa\pi}{2}-2\lambda_3} \mathrm{d}\lambda_2 \int_0^{\kappa\pi} \mathrm{d}\lambda_1 \int_{-M_-}^{M_-} \mathrm{d}\lambda_4 \, \mathcal{B}[\lambda_1,\lambda_2,\lambda_3,\lambda_4] \\
& + \int_{-\frac{\kappa\pi}{3}}^{-3\frac{\kappa\pi}{10}} \mathrm{d}\lambda_3 \int_{-\lambda_3}^{\frac{\kappa\pi}{2}+\frac{\lambda_3}{2}} \mathrm{d}\lambda_2 \int_0^{\kappa\pi} \mathrm{d}\lambda_1 \int_{-M_+}^{M_+} \mathrm{d}\lambda_4 \, \mathcal{B}[\lambda_1,\lambda_2,\lambda_3,\lambda_4] \\
& + \int_{-3\frac{\kappa\pi}{10}}^{-(1+3\kappa)\frac{\pi}{30}} \mathrm{d}\lambda_3 \int_{-\lambda_3}^{\frac{\kappa\pi}{8}-\frac{3\lambda_3}{4}} \mathrm{d}\lambda_2 \int_0^{\kappa\pi} \mathrm{d}\lambda_1 \int_{-M_+}^{M_+} \mathrm{d}\lambda_4 \, \mathcal{B}[\lambda_1,\lambda_2,\lambda_3,\lambda_4] \\
& + \int_{-(1+3\kappa)\frac{\pi}{30}}^{-\frac{\pi}{24}} \mathrm{d}\lambda_3 \left\{ \int_{-\lambda_3}^{-\frac{\pi}{24}-2\lambda_3} \mathrm{d}\lambda_2 \int_0^{\kappa\pi} \mathrm{d}\lambda_1 \int_{-M_+}^{M_+} \mathrm{d}\lambda_4 \, \mathcal{B}[\lambda_1,\lambda_2,\lambda_3,\lambda_4] \right. \\
& \qquad \left. + \int_{-\frac{\pi}{24}-2\lambda_3}^{\frac{\kappa\pi}{8}-\frac{3\lambda_3}{4}} \mathrm{d}\lambda_2 \int_0^{\kappa\pi} \mathrm{d}\lambda_1 \int_{-M_-}^{M_-} \mathrm{d}\lambda_4 \, \mathcal{B}[\lambda_1,\lambda_2,\lambda_3,\lambda_4] \right\} \\
& + \int_{-\frac{\pi}{24}}^{0} \mathrm{d}\lambda_3 \int_{-\lambda_3}^{\frac{\kappa\pi}{8}-3\frac{\lambda_3}{4}} \mathrm{d}\lambda_2 \int_0^{\kappa\pi} \mathrm{d}\lambda_1 \int_{-M_-}^{M_-} \mathrm{d}\lambda_4 \, \mathcal{B}[\lambda_1,\lambda_2,\lambda_3,\lambda_4].
\end{aligned}$$

Here $\mathcal{B}[\lambda_1,\lambda_2,\lambda_3,\lambda_4]$ denotes the Boolean function for the remaining relevant constraints Eqs.(B6,B8,B9,B11 B13).

In the $\lambda_1 < 0$ part one has to take also into account that Eq.(B10) reduces to its first

inequality for $\lambda_3 < 0$, and to its second inequality for $\lambda_3 > 0$. V_- can then be written as,

$$
\begin{aligned}
V_- \;=\; & \int_0^{\frac{3\kappa\pi}{10}} \mathrm{d}\lambda_3 \int_{-\frac{\lambda_3}{2}}^{\frac{\kappa\pi}{8}-\frac{3\lambda_3}{4}} \mathrm{d}\lambda_2 \int_{-\sqrt{\lambda_2+\frac{\lambda_3}{2}}\sqrt{\frac{\pi}{6}}}^{0} \mathrm{d}\lambda_1 \int_{-M_-}^{M_-} \mathrm{d}\lambda_4\, \mathcal{B}[\lambda_1,\lambda_2,\lambda_3,\lambda_4] \\
& + \int_{\frac{3\kappa\pi}{10}}^{\frac{\kappa\pi}{3}} \mathrm{d}\lambda_3 \int_{-\frac{\lambda_3}{2}}^{\frac{\kappa\pi}{2}-2\lambda_3} \mathrm{d}\lambda_2 \int_{-\sqrt{\lambda_2+\frac{\lambda_3}{2}}\sqrt{\frac{\pi}{6}}}^{0} \mathrm{d}\lambda_1 \int_{-M_-}^{M_-} \mathrm{d}\lambda_4\, \mathcal{B}[\lambda_1,\lambda_2,\lambda_3,\lambda_4] \\
& + \int_{-\frac{\kappa\pi}{3}}^{-3\frac{\kappa\pi}{10}} \mathrm{d}\lambda_3 \int_{-\lambda_3}^{\frac{\kappa\pi}{2}+\frac{\lambda_3}{2}} \mathrm{d}\lambda_2 \int_{-\sqrt{\lambda_2+\lambda_3}\sqrt{\frac{\pi}{6}}}^{0} \mathrm{d}\lambda_1 \int_{-M_+}^{M_+} \mathrm{d}\lambda_4\, \mathcal{B}[\lambda_1,\lambda_2,\lambda_3,\lambda_4] \\
& + \int_{-3\frac{\kappa\pi}{10}}^{-(1+3\kappa)\frac{\pi}{30}} \mathrm{d}\lambda_3 \int_{-\lambda_3}^{\frac{\kappa\pi}{8}-\frac{3\lambda_3}{4}} \mathrm{d}\lambda_2 \int_{-\sqrt{\lambda_2+\lambda_3}\sqrt{\frac{\pi}{6}}}^{0} \mathrm{d}\lambda_1 \int_{-M_+}^{M_+} \mathrm{d}\lambda_4\, \mathcal{B}[\lambda_1,\lambda_2,\lambda_3,\lambda_4] \\
& + \int_{-(1+3\kappa)\frac{\pi}{30}}^{-\frac{\pi}{24}} \mathrm{d}\lambda_3 \left\{ \int_{-\lambda_3}^{-\frac{\pi}{24}-2\lambda_3} \mathrm{d}\lambda_2 \int_{-\sqrt{\lambda_2+\lambda_3}\sqrt{\frac{\pi}{6}}}^{0} \mathrm{d}\lambda_1 \int_{-M_+}^{M_+} \mathrm{d}\lambda_4\, \mathcal{B}[\lambda_1,\lambda_2,\lambda_3,\lambda_4] \right. \\
& \qquad \left. + \int_{-\frac{\pi}{24}-2\lambda_3}^{\frac{\kappa\pi}{8}-\frac{3\lambda_3}{4}} \mathrm{d}\lambda_2 \int_{-\sqrt{\lambda_2+\frac{\lambda_3}{2}}\sqrt{\frac{\pi}{6}}}^{0} \mathrm{d}\lambda_1 \int_{-M_-}^{M_-} \mathrm{d}\lambda_4\, \mathcal{B}[\lambda_1,\lambda_2,\lambda_3,\lambda_4] \right\} \\
& + \int_{-\frac{\pi}{24}}^{0} \mathrm{d}\lambda_3 \int_{-\lambda_3}^{\frac{\kappa\pi}{8}-3\frac{\lambda_3}{4}} \mathrm{d}\lambda_2 \int_{-\sqrt{\lambda_2+\lambda_3}\sqrt{\frac{\pi}{6}}}^{0} \mathrm{d}\lambda_1 \int_{-M_-}^{M_-} \mathrm{d}\lambda_4\, \mathcal{B}[\lambda_1,\lambda_2,\lambda_3,\lambda_4]
\end{aligned}
$$

We stress that the same Boolean function $\mathcal{B}$ operates in both $V_\pm$ domains. The reason is that the would-be extra constraint $-\kappa\pi < \lambda_1$ of Eq.(B7) relevant for V_- can be shown to be always satisfied in the (λ_2, λ_3) domain defined by Eqs.(B2 - B5) when combined with Eqs.(B10). We note also that $\mathcal{B}$ can be explicitly traded for further multiple piecewise integrations in the (λ_1, λ_4), leading to highly involved but fully analytical integrations. We refrain though from doing this here, since we are only interested in a numerical estimate of the hyper-volumes. The above forms of V_+ and V_- lend themselves easily to such an estimate upon use of packages such as Mathematica.

More general sub-volumes such as $V_+^{\lambda_1>\lambda_1^{min}>0}$ or $V_-^{\lambda_1<\lambda_1^{max}<0}$, can be obtained respectively from V_+ through the substitution $\int_0^{\kappa\pi} \mathrm{d}\lambda_1 \to \int_{\lambda_1^{min}}^{\kappa\pi} \mathrm{d}\lambda_1$, and from V_- through the substitutions $\int_{-\sqrt{\lambda_2+\frac{\lambda_3}{2}}\sqrt{\frac{\pi}{6}}}^{0} \mathrm{d}\lambda_1 \to \int_{-\sqrt{\lambda_2+\frac{\lambda_3}{2}}\sqrt{\frac{\pi}{6}}}^{\lambda_1^{max}} \mathrm{d}\lambda_1$ and $\int_{-\sqrt{\lambda_2+\lambda_3}\sqrt{\frac{\pi}{6}}}^{0} \mathrm{d}\lambda_1 \to \int_{-\sqrt{\lambda_2+\lambda_3}\sqrt{\frac{\pi}{6}}}^{\lambda_1^{max}} \mathrm{d}\lambda_1$.

The results of the numerical evaluation using Mathematica are given in table VI.

Appendix C: QCD corrections to Higgs hadronic decays

Hereafter m denotes generically the h^0, A^0 masses. We implemented the running quark masses $\overline{m}_b(\mu)$, $\overline{m}_c(\mu)$ as well as $\alpha_s(\mu)$ up to 4-loop QCD order, relying partly on [76] and

κ	8	16
V_+	2514	39796
V_-	275	3027
$V_+^{\lambda_1>10}$	273	18439
$V_-^{\lambda_1<-0.5}$	92	1517
$V_-^{\lambda_1<-1}$	7	433

TABLE VI: Sizes of the various sub-volumes in the U-BFB four dimensional λ_i parameter space region, for $\kappa = 8, 16$ and $\lambda = \frac{\pi}{6}$.

partly on our private code, fixing the $\overline{\rm MS}$ b- and c-quark masses to $\overline{m}_b(m_b) = m_b = 4.16$GeV, $\overline{m}_c(m_c) = m_c = 1.28$GeV, and $\overline{\alpha}_s(M_Z) = 0.1184$ with $M_Z = 91.18$GeV. The b- and c-quark pole masses are taken $M_b = 4.69$GeV, $M_c = 1.55$GeV, and the top quark mass $M_t = 173$GeV. The other relevant parameters are fixed as follows: $M_\tau = 1.777$GeV, $G_F = 1.16637 \times 10^{-5}\text{GeV}^{-2}$, $v_d = 246$GeV.

-$b\bar{b}$ decay widths of h^0, A^0: we use here the results of [77],

$$\begin{aligned}\Gamma_{S\to b\bar{b}} \;=\; & \frac{3G_F}{4\sqrt{2}\pi} C_{bb}^S \, m_S \, \overline{m}_b^2(m_S)\Big(1 + \Delta\Gamma_{1,S}\frac{\overline{\alpha}_s(m_S)}{\pi} + (\Delta\Gamma_{2,S} + \frac{m_S^2}{M_t^2}\Delta\tilde{\Gamma}_{2,S})\frac{\overline{\alpha}_s^2(m_S)}{\pi^2} \\ & + \frac{\overline{m}_b^2(m_S)}{m_S^2}\big(\Delta\Gamma_0^{(m_S)} + \Delta\Gamma_1^{(m_S)}\frac{\overline{\alpha}_s(m_S)}{\pi} + (\Delta\Gamma_2^{(m_S)} + \frac{m_S^2}{M_t^2}\Delta\tilde{\Gamma}_2^{(m_S)})\frac{\overline{\alpha}_s^2(m_S)}{\pi^2}\big) \\ & + \mathcal{O}(\frac{\overline{m}_b^4(m_S)}{m_S^4})\Big) \end{aligned} \tag{C1}$$

with $S = h^0, A^0$ and

$$
\begin{aligned}
\Delta\Gamma_{1,h^0} &= \frac{17}{3} \\
\Delta\Gamma_{2,h^0} &= 29.147 + k_{h^0}\big(1.57 - \frac{2}{3}\ln[\frac{m_{h^0}^2}{M_t^2}] + \frac{1}{9}\ln^2[\frac{\overline{m}_b^2(m_{h^0})}{m_{h^0}^2}]\big) \\
\Delta\tilde{\Gamma}_{2,h^0} &= \frac{107}{675} - \frac{2}{45}\ln[\frac{m_{h^0}^2}{M_t^2}] + k_{h^0}\big(-0.007 - \frac{41}{1620}\ln[\frac{m_{h^0}^2}{M_t^2}] + \frac{7}{1080}\ln^2[\frac{\overline{m}_b^2(m_{h^0})}{m_{h^0}^2}]\big) \\
\Delta\Gamma_0^{(m_{h^0})} &= -6 \\
\Delta\Gamma_1^{(m_{h^0})} &= -40 \\
\Delta\Gamma_2^{(m_{h^0})} &= -107.755 - 0.98\ln^2[\frac{\overline{m}_b^2(m_{h^0})}{m_{h^0}^2}] - \frac{1}{12}\ln^4[\frac{\overline{m}_b^2(m_{h^0})}{m_{h^0}^2}] + 4 \\
&\quad + k_{h^0}\big(-5.61 + 4\ln[\frac{m_{h^0}^2}{M_t^2}] + \frac{16}{9}\ln[\frac{\overline{m}_b^2(m_{h^0})}{m_{h^0}^2}] - \frac{4}{9}\ln^2[\frac{\overline{m}_b^2(m_{h^0})}{m_{h^0}^2}]\big) \\
\Delta\tilde{\Gamma}_2^{(m_{h^0})} &= -\frac{116}{75} + \frac{8}{45}\ln[\frac{m_{h^0}^2}{M_t^2}] \\
&\quad + k_{h^0}\big(0.52 - \frac{7}{270}\ln[\frac{m_{h^0}^2}{M_t^2}] + \frac{1}{135}\ln[\frac{\overline{m}_b^2(m_{h^0})}{m_{h^0}^2}] - \frac{7}{270}\ln^2[\frac{\overline{m}_b^2(m_{h^0})}{m_{h^0}^2}]\big) \\
\Delta\Gamma_{1,A^0} &= \frac{17}{3} \\
\Delta\Gamma_{2,A^0} &= 29.147 + k_{A^0}\big(\frac{23}{6} - \ln[\frac{m_{A^0}^2}{M_t^2}] + \frac{1}{6}\ln^2[\frac{\overline{m}_b^2(m_{A^0})}{m_{A^0}^2}]\big) \\
\Delta\tilde{\Gamma}_{2,A^0} &= \frac{107}{675} - \frac{2}{45}\ln[\frac{m_{A^0}^2}{M_t^2}] + k_{A^0}\big(0.051 - \frac{7}{108}\ln[\frac{m_{A^0}^2}{M_t^2}] + \frac{1}{72}\ln[\frac{\overline{m}_b^2(m_{A^0})}{m_{A^0}^2}]^2\big) \\
\Delta\Gamma_0^{(m_{A^0})} &= -2 \\
\Delta\Gamma_1^{(m_{A^0})} &= -\frac{8}{3} \\
\Delta\Gamma_2^{(m_{A^0})} &= 91.006 - 26.32\ln^2[\frac{\overline{m}_b^2(m_{A^0})}{m_{A^0}^2}] - \frac{4}{3}\ln^4[\frac{\overline{m}_b^2(m_{A^0})}{m_{A^0}^2}] + 4 \\
&\quad + k_{A^0}\big(-5 + 2\ln[\frac{m_{A^0}^2}{M_t^2}] - \frac{4}{3}\ln[\frac{\overline{m}_b^2(m_{A^0})}{m_{A_0}^2}]\big) \\
\Delta\tilde{\Gamma}_2^{(m_{A^0})} &= -\frac{16}{25} + \frac{4}{15}\ln[\frac{m_{A^0}^2}{M_t^2}] + k_{A^0}\big(\frac{19}{108} - \frac{1}{18}\ln[\frac{m_{A^0}^2}{M_t^2}] - \frac{2}{9}\ln[\frac{\overline{m}_b^2(m_{A^0})}{m_{A^0}^2}]\big) \qquad \text{(C2)}
\end{aligned}
$$

In the above, the number of quark flavors, $n_f = 5$, has been assumed in the widths and in the running quantities, since $m_b \ll m_S < m_t$.

-$c\bar{c}$ decay widths of h^0, A^0: these can be read from Eqs.(C1) to (C2) by discarding the extra contributions of finite c-quark mass, as well as those originating from the heavy top limit [77],

$$\Gamma_{S\to c\bar{c}} \;=\; \frac{3G_F}{4\sqrt{2}\pi}C_{cc}^S\, m_S\, \overline{m}_c^2(m_S)\big(1+5.67\frac{\overline{\alpha}_s(m_S)}{\pi}+(35.94-1.36n_f+\delta_{c\bar{c}}^S)\frac{\overline{\alpha}_s^2(m_S)}{\pi^2}+\mathcal{O}(\frac{\overline{\alpha}_s^3(m_S)}{\pi^3})\,\big)$$

where

$$\begin{aligned}\delta_{c\bar{c}}^{h^0} \;&=\; k_{h^0}(1.57-\frac{2}{3}\ln[\frac{m_{h^0}^2}{M_t^2}]+\frac{1}{9}\ln^2[\frac{\overline{m}_c^2(m_{h^0})}{m_{h^0}^2}])\\ \delta_{c\bar{c}}^{A^0} \;&=\; k_{A^0}(\frac{23}{6}-\ln[\frac{m_{A^0}^2}{M_t^2}]+\frac{1}{6}\ln^2[\frac{\overline{m}_c^2(m_{A^0})}{m_{A^0}^2}])\end{aligned}$$

where again one should take $n_f = 5$. Note that another known mass-independent $\mathcal{O}(\alpha_s^3)$ correction, $\delta_{c\bar{c}}^{(3)} = (164.14-25.77n_f+0.26n_f^2)\frac{\overline{\alpha}_s^3(m)}{\pi^3}$, has not been included as it does not give significant contributions (see for instance [37] for a review of the QCD effects).

-decay widths of h^0, A^0 in two gluons in the limit $m \ll M_t$: we use the results of [78],

$$\Gamma_{S\to gg} = \Gamma_{S\to gg}^{\rm LO} K_{\rm factor}(n_f, m_S); \tag{C3}$$

$$\Gamma_{S\to gg}^{LO} = c_S C^S \frac{G_F m^3}{36\sqrt{2}\pi}\frac{\overline{\alpha}_s^2(m_S)}{\pi^2} \tag{C4}$$

with

$$c_{h^0} = 1, \quad c_{A^0} = 4 \tag{C5}$$

$$\begin{aligned}K_{\rm factor}(n_f,\mu) \;=\; 1+\frac{\overline{\alpha}_s(m)}{\pi}\big(\frac{95}{4}-\frac{7}{6}n_f\big)+\frac{\overline{\alpha}_s^2(m)}{\pi^2}\big(\frac{149533}{288}-\frac{363}{8}\zeta(2)-\frac{495}{8}\zeta(3)-\frac{19}{8}\ln[\frac{M_t^2}{\mu^2}]\\ +n_f(-\frac{4157}{72}+\frac{11}{2}\zeta(2)+\frac{5}{4}\zeta(3)-\frac{2}{3}\ln[\frac{M_t^2}{\mu^2}])+n_f^2(\frac{127}{108}-\frac{1}{6}\zeta(2))\big)+\mathcal{O}(\frac{\overline{\alpha}_s^3(m)}{\pi^3})\end{aligned}$$

with $\zeta(2) = \pi^2/6$ and $\zeta(3) \simeq 1.20206$.

The coefficients $C_{ff'}^S$, being defined as the product of the reduced couplings of f and f' to S, and k_S defined as the ratios of these products, one has in the case of H^0*-scenario* under consideration, see table II,

$$\begin{aligned}&C_{bb}^{h_0} = C_{cc}^{h_0} = C^{h_0} = \frac{(\lambda_1+\lambda_4)^2}{\lambda^2}\times\frac{4v_t^2}{v_d^2},\\ &C_{bb}^{A_0} = C_{cc}^{A_0} = C^{A_0} = \frac{4v_t^2}{v_d^2},\\ &k_{h^0} = k_{A^0} = 1.\end{aligned}$$

Appendix D: relevant cross-section, width, decay length

For completness we recall here the tree-level expressions of the Z-boson decay width into a scalar and a pseudo-scalar states, as well as the $e^+e^- \to h^0A^0$ cross-section for a generic properly normalized coupling c, see also section V,

$$\Gamma_{Z\to h^0A^0} = \frac{c^2\sqrt{2}G_F m_Z^3}{48\pi} \times \lambda[1, \frac{m_{h^0}^2}{m_Z^2}, \frac{m_{A^0}^2}{m_Z^2}]^{\frac{3}{2}} \tag{D1}$$

$$\sigma(e^+e^- \to h^0A^0) = \frac{c^2G_F^2 m_Z^4}{96\pi s}(1+(1-4s_W^2)^2) \times (1-\frac{m_Z^2}{s})^{-2}\lambda[1, \frac{m_{h^0}^2}{s}, \frac{m_{A^0}^2}{s}]^{\frac{3}{2}} \tag{D2}$$

with the usual phase-space function defined as

$$\lambda[x, y^2, z^2] \equiv (x-(y-z)^2)(x-(y+z)^2)$$

The decay length $c\tau$ in the laboratory frame for a particle of mass m, energy $E = \frac{\sqrt{s}}{2}$ and total decay width Γ, is given, in the instantaneous decay approximation, by

$$c\tau = 9.86 \times 10^{-17} \times \frac{(s-4\,m^2)^{\frac{1}{2}}}{m\,\Gamma} \tag{D3}$$

where mass, energy and width are in GeV and $c\tau$ in meters.

---

[1] ATLAS Collaboration, G. Aad *et al.*, Phys.Lett. **B716**, 1 (2012), 1207.7214.

[2] CMS Collaboration, S. Chatrchyan *et al.*, Phys.Lett. **B716**, 30 (2012), 1207.7235.

[3] ATLAS-CONF-2013-034, (2013).

[4] CMS-PAS-HIG-13-005, (2013).

[5] ATLAS-CONF-2013-040, (2013).

[6] CMS-PAS-HIG-13-002, (2013).

[7] CMS-PAS-HIG-13-003, (2013).

[8] ATLAS Collaboration, G. Aad *et al.*, (2014), 1406.3827.

[9] CMS Collaboration, V. Khachatryan *et al.*, (2014), 1407.0558.

[10] W. Konetschny and W. Kummer, Phys. Lett. **B70**, 433 (1977).

[11] T. P. Cheng and L.-F. Li, Phys. Rev. **D22**, 2860 (1980).

[12] G. Lazarides, Q. Shafi, and C. Wetterich, Nucl. Phys. **B181**, 287 (1981).

[13] J. Schechter and J. W. F. Valle, Phys. Rev. **D22**, 2227 (1980).

[14] R. N. Mohapatra and G. Senjanovic, Phys. Rev. **D23**, 165 (1981).

[15] A. Arhrib *et al.*, Phys.Rev. **D84**, 095005 (2011), 1105.1925.

[16] A. Akeroyd and S. Moretti, Phys.Rev. **D86**, 035015 (2012), 1206.0535.

[17] L. Wang and X.-F. Han, Phys.Rev. **D87**, 015015 (2013), 1209.0376.

[18] A. Akeroyd, M. Aoki, and H. Sugiyama, (2011).

[19] M. Aoki, S. Kanemura, and K. Yagyu, Phys.Rev. **D85**, 055007 (2012), 1110.4625.

[20] P. Bhupal Dev, D. K. Ghosh, N. Okada, and I. Saha, JHEP **1303**, 150 (2013), 1301.3453.

[21] A. G. Akeroyd and C.-W. Chiang, Phys. Rev. **D81**, 115007 (2010), 1003.3724.

[22] P. Fileviez Perez, T. Han, G.-y. Huang, T. Li, and K. Wang, Phys. Rev. **D78**, 015018 (2008), 0805.3536.

[23] LHC Higgs Cross Section Working Group, A. David *et al.*, (2012), 1209.0040.

[24] CMS Collaboration, (2013), 1307.7135.

[25] ATL-PHYS-PUB-2013-014.

[26] Particle Data Group, K. Nakamura *et al.*, J.Phys.G **G37**, 075021 (2010).

[27] S. Kanemura and K. Yagyu, Phys.Rev. **D85**, 115009 (2012), 1201.6287.

[28] S. Kanemura and H. Sugiyama, Phys.Rev. **D86**, 073006 (2012), 1202.5231.

[29] R. Franceschini and R. Mohapatra, (2013), 1306.6108.

[30] T. Banks and N. Seiberg, Phys.Rev. **D83**, 084019 (2011), 1011.5120.

[31] ATLAS-CONF-2013-012.

[32] CMS-PAS-HIG-13-001.

[33] A. Arhrib, R. Benbrik, M. Chabab, G. Moultaka, and L. Rahili, JHEP **1204**, 136 (2012), 1112.5453.

[34] R. Cahn, M. S. Chanowitz, and N. Fleishon, Phys.Lett. **B82**, 113 (1979).

[35] L. Bergstrom and G. Hulth, Nucl.Phys. **B259**, 137 (1985); Erratum-ibid. **B276**, 744 (1986).

[36] J. F. Gunion, H. E. Haber, G. L. Kane, and S. Dawson, Front.Phys. **80**, 1 (2000).

[37] M. Spira, Fortsch. Phys. **46**, 203 (1998), hep-ph/9705337.

[38] A. Djouadi, Phys. Rept. **459**, 1 (2008), hep-ph/0503173.

[39] C.-S. Chen, C.-Q. Geng, D. Huang, and L.-H. Tsai, (2013), 1302.0502.

[40] C.-S. Chen, C.-Q. Geng, D. Huang, and L.-H. Tsai, (2013), 1301.4694.

[41] T. Hahn, Comput. Phys. Commun. **140**, 418 (2001), hep-ph/0012260.

[42] T. Hahn and M. Perez-Victoria, Comput. Phys. Commun. **118**, 153 (1999), hep-ph/9807565.

[43] ATLAS Collaboration, G. Aad *et al.*, Eur.Phys.J. **C72**, 2244 (2012), 1210.5070.

[44] CMS Collaboration, S. Chatrchyan *et al.*, Eur.Phys.J. **C72**, 2189 (2012), 1207.2666.

[45] ATLAS-CONF-2013-009, (2013).

[46] ATLAS Collaboration, G. Aad *et al.*, Phys.Lett. **B732**, 8 (2014), 1402.3051.

[47] CMS Collaboration, S. Chatrchyan *et al.*, (2013), 1307.5515.

[48] A. Melfo, M. Nemevsek, F. Nesti, G. Senjanovic, and Y. Zhang, (2011), 1108.4416.

[49] CMS Collaboration, S. Chatrchyan *et al.*, JHEP **06**, 081 (2013), 1303.4571.

[50] ATLAS-CONF-2012-079, (2012).

[51] ATLAS Collaboration, G. Aad *et al.*, Phys.Rev.Lett. **112**, 201802 (2014), 1402.3244.

[52] CMS Collaboration, CMS-PAS-HIG-13-018, (2013).

[53] CMS Collaboration, CMS-PAS-HIG-13-013, (2013).

[54] CMS Collaboration, S. Chatrchyan *et al.*, Eur.Phys.J. **C74**, 2980 (2014), 1404.1344.

[55] C. Englert, T. Plehn, M. Rauch, D. Zerwas, and P. M. Zerwas, Phys.Lett. **B707**, 512 (2012), 1112.3007.

[56] K. Cheung, J. S. Lee, and P.-Y. Tseng, JHEP **1305**, 134 (2013), 1302.3794.

[57] G. Belanger, B. Dumont, U. Ellwanger, J. Gunion, and S. Kraml, Phys.Lett. **B723**, 340 (2013), 1302.5694.

[58] G. Belanger, B. Dumont, U. Ellwanger, J. Gunion, and S. Kraml, Phys.Rev. **D88**, 075008 (2013), 1306.2941.

[59] J. R. Espinosa, M. Muhlleitner, C. Grojean, and M. Trott, JHEP **1209**, 126 (2012), 1205.6790.

[60] C. Englert, M. Spannowsky, and C. Wymant, Phys.Lett. **B718**, 538 (2012), 1209.0494.

[61] BESIII Collaboration, M. Ablikim *et al.*, Phys.Rev. **D85**, 092012 (2012), 1111.2112.

[62] BaBar collaboration, J. Lees *et al.*, Phys.Rev. **D87**, 031102 (2013), 1210.0287.

[63] BaBar Collaboration, J. Lees *et al.*, Phys.Rev. **D88**, 031701 (2013), 1307.5306.

[64] CMS-PAS-HIG-13-007, (2013).

[65] ATLAS-CONF-2013-010, ATLAS-COM-CONF-2013-003, (2013).

[66] OPAL Collaboration, G. Abbiendi *et al.*, Eur.Phys.J. **C18**, 425 (2001), hep-ex/0007040.

[67] DELPHI, J. Abdallah *et al.*, Eur. Phys. J. **C38**, 1 (2004), hep-ex/0410017.

[68] OPAL Collaboration, G. Abbiendi *et al.*, Eur.Phys.J. **C40**, 317 (2005), hep-ex/0408097.

[69] LEP Higgs Working Group, ALEPH collaboration, DELPHI collaboration, L3 collaboration, OPAL Collaboration, (2001), hep-ex/0107030.

[70] Particle Data Group, J. Beringer *et al.*, Phys.Rev. **D86**, 010001 (2012).

[71] OPAL Collaboration, K. Ackerstaff *et al.*, Eur.Phys.J. **C5**, 19 (1998), hep-ex/9803019.

[72] OPAL Collaboration, K. Ackerstaff *et al.*, Eur.Phys.J. **C1**, 425 (1998), hep-ex/9709003.

[73] S. Kanemura, K. Yagyu, and H. Yokoya, Phys.Lett. **B726**, 316 (2013), 1305.2383.

[74] Z. Kang, J. Li, T. Li, Y. Liu, and G.-Z. Ning, (2014), 1404.5207.

[75] S. Kanemura, M. Kikuchi, K. Yagyu, and H. Yokoya, (2014), 1407.6547.

[76] K. Chetyrkin, J. H. Kuhn, and M. Steinhauser, Comput.Phys.Commun. **133**, 43 (2000), hep-ph/0004189.

[77] K. Chetyrkin and A. Kwiatkowski, Nucl.Phys. **B461**, 3 (1996), hep-ph/9505358.

[78] K. Chetyrkin, B. A. Kniehl, and M. Steinhauser, Phys.Rev.Lett. **79**, 353 (1997), hep-ph/9705240.

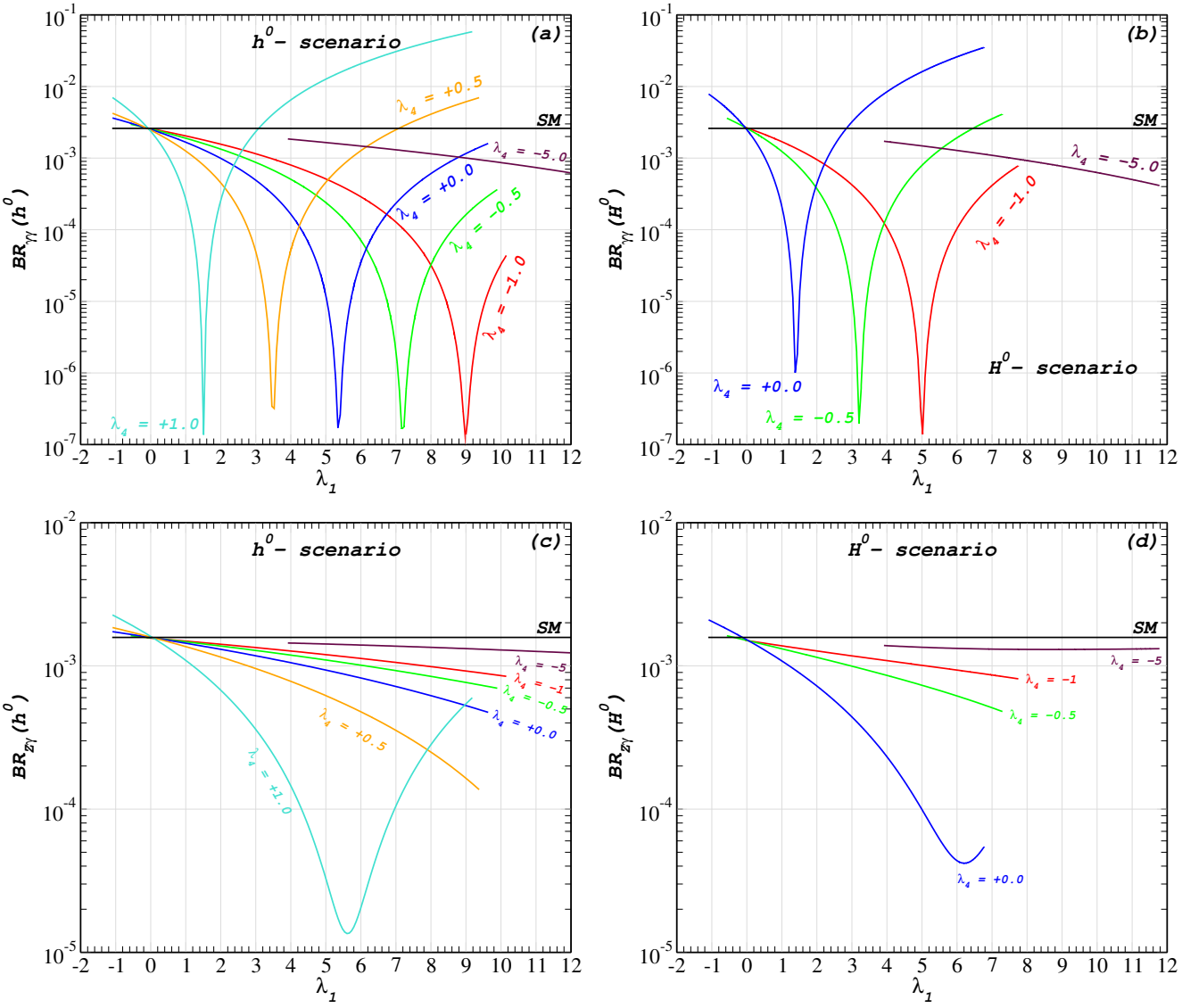

FIG. 2: The $\mathcal{H} \to \gamma\gamma, Z\gamma$ branching ratios as a function of λ_1 for various values of λ_4. We take $\lambda_3 = 2\lambda_2$, $-5 \leq \lambda_2 \leq 5$, $-2 \leq \lambda_1 \leq 12$ and $v_t = 1$ GeV. figures (a),(c): 'h^0*scenario*', $\mu = 1$ GeV, $\lambda = 0.521$, $m_{h^0} = 125$–125.6 GeV, $m_{H^0} \simeq m_{A^0} \approx 207$ GeV, 162 GeV $\lesssim m_{H^+} \lesssim 474$ GeV, 97 GeV $\lesssim m_{H^{++}} \lesssim 637$ GeV and $0.9 \leq \cos\alpha \leq 1$; figures (b),(d): '$H^0$*scenario*', $\mu = 0.3$ GeV, $m_{H^0} = 125$–126.5 GeV, with λ as given by Eq. (2.23), $m_{h^0} \simeq m_{A^0} \approx 113$ GeV, 100 GeV $\lesssim m_{H^+} \lesssim 440$ GeV, 100 GeV $\lesssim m_{H^{++}} \lesssim 612$ GeV and $0.9 \leq |\sin\alpha| \leq 1$.

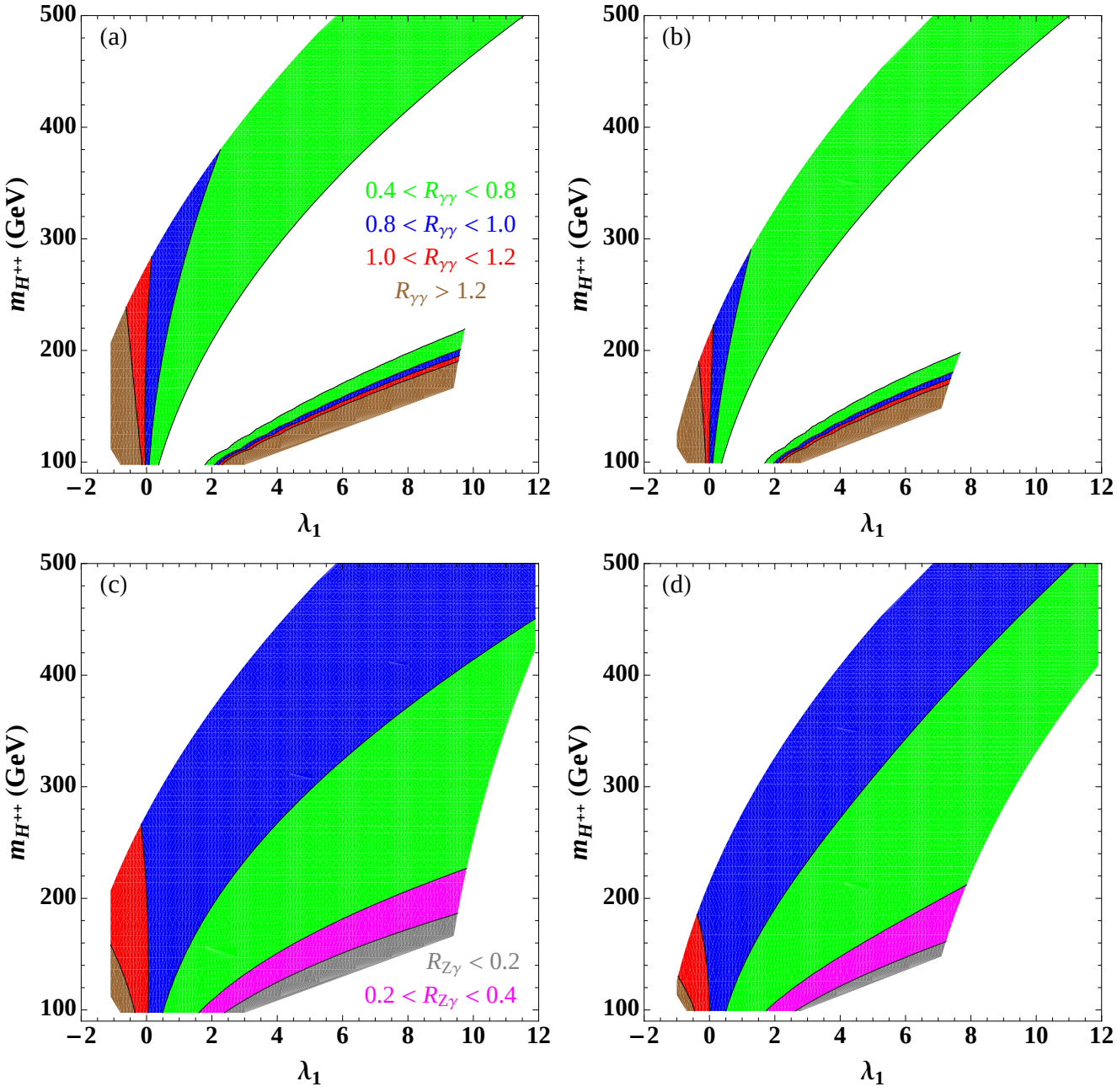

FIG. 3: Scatter plots in the $[\lambda_1, m_{H^{++}}]$ showing the ratios $R_{\gamma\gamma}$ (upper) and $R_{Z\gamma}$ (lower). (a), (c) correspond to the 'h^0*scenario*' and (b), (d) to the 'H^0*scenario*'. The color code is the same for the four figures. The scan is in the range $-12 \leq \lambda_4 \leq 2$ and all other parameter and mass values are as in Fig.2

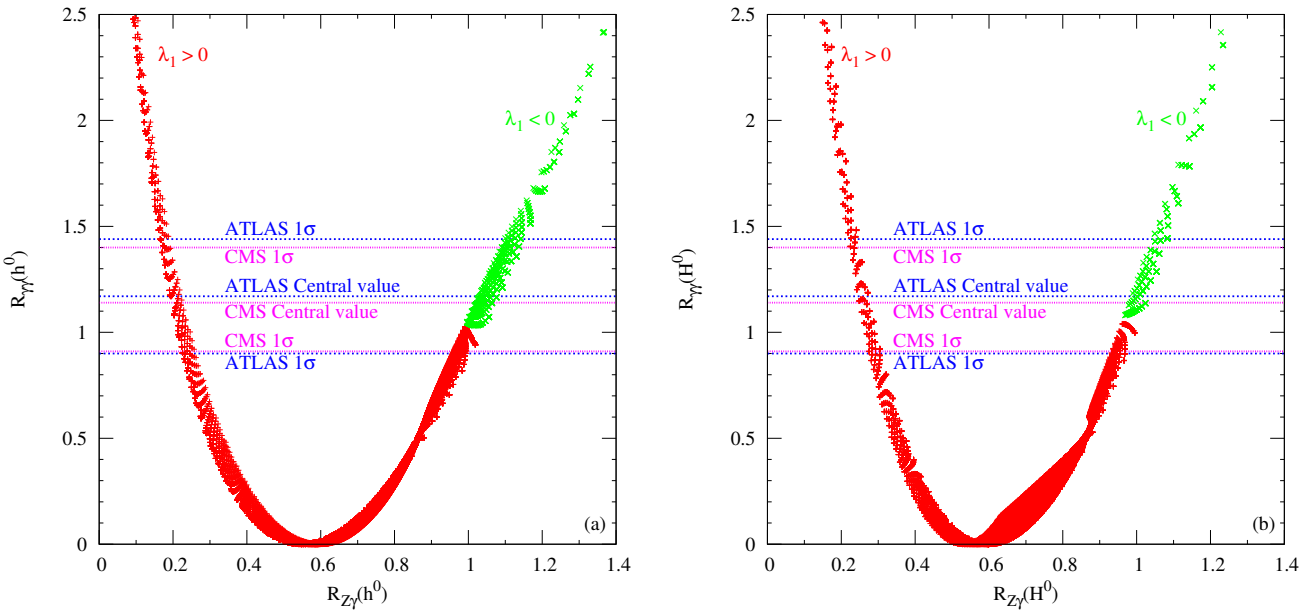

FIG. 4: Correlation between $R_{Z\gamma}$ and $R_{\gamma\gamma}$ observables, (a) 'h^0*scenario*', (b) 'H^0*scenario*'; the parameter scan and mass ranges are as in Figs.2, 3; the scatter points correspond to $\lambda_1 < 0$ (green) and $\lambda_1 > 0$ (red). We also show the central values and 1σ bands of the recent ATLAS [8] and CMS [9] results. See text for further discussion.

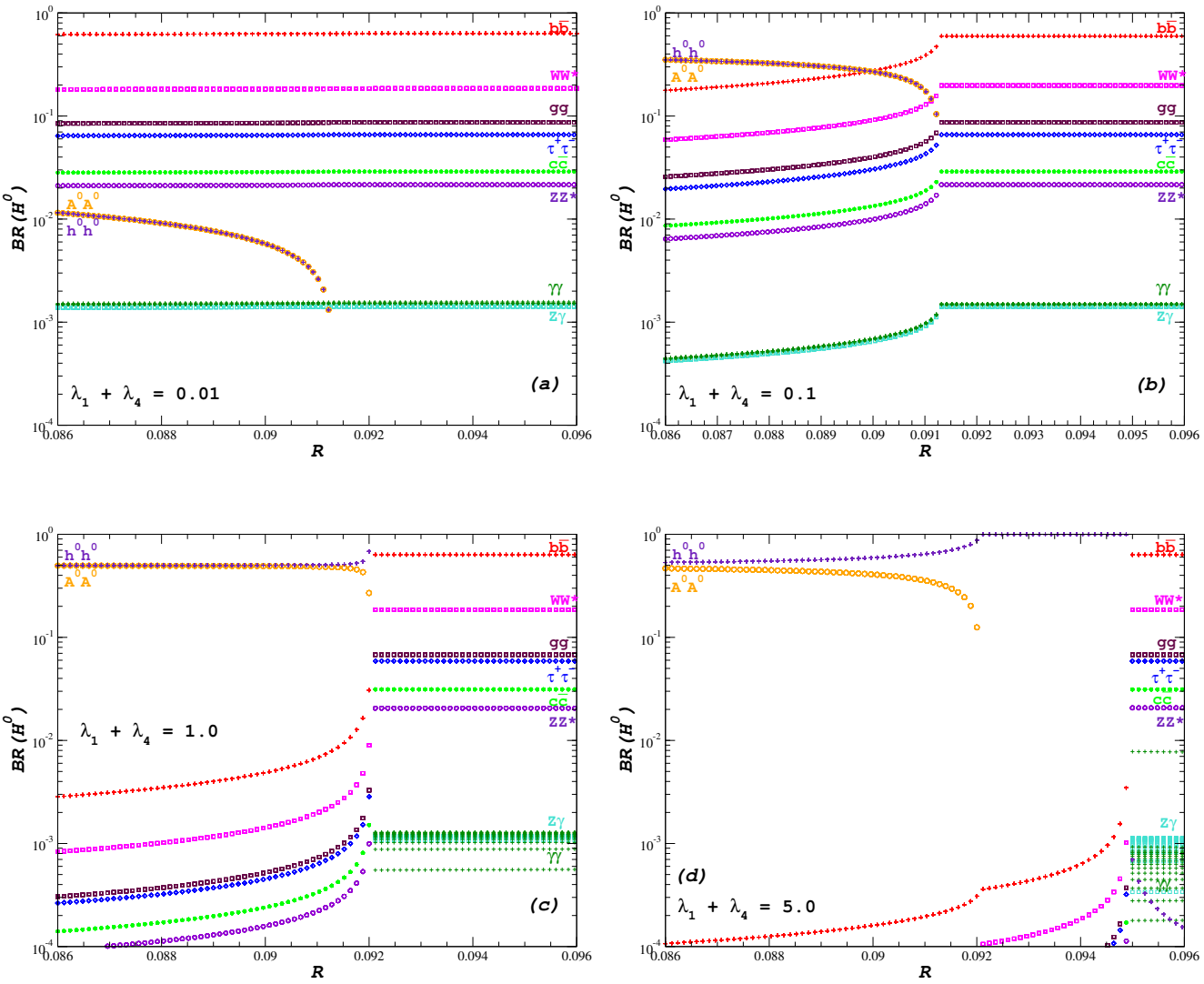

FIG. 5: The branching ratios $BR(H^0)$ as a function of the ratio $R \equiv \frac{\mu}{v_t}$, for $m_{H^0} = 125.5$ GeV, $\lambda_2 = 0.1$, $\lambda_3 = 2\lambda_2$, $-10 \leq \lambda_4 \leq 2$ and various values of $\lambda_1 + \lambda_4$.

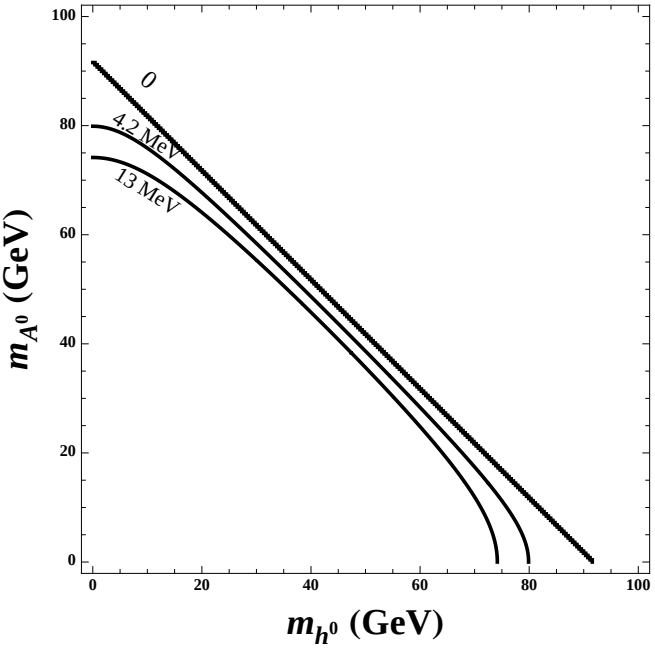

FIG. 6: constraint from the $Z \to h^0 A^0$ contribution to the Z-boson total width.

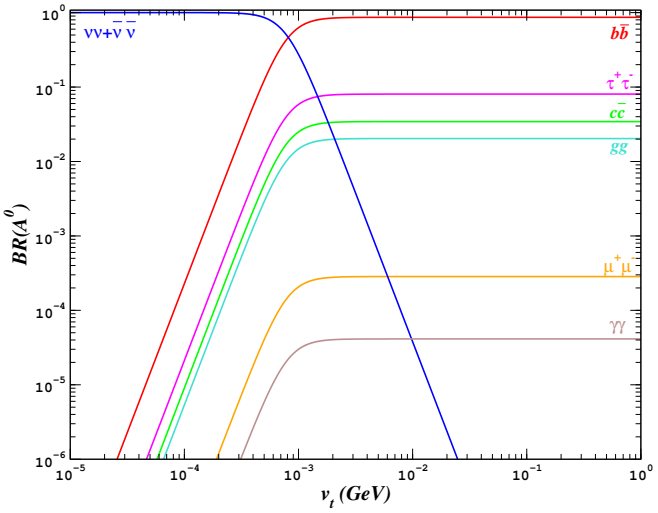

FIG. 7: Branching ratios of A^0 as a function of v_t for $m_{A^0} \approx 55$GeV.

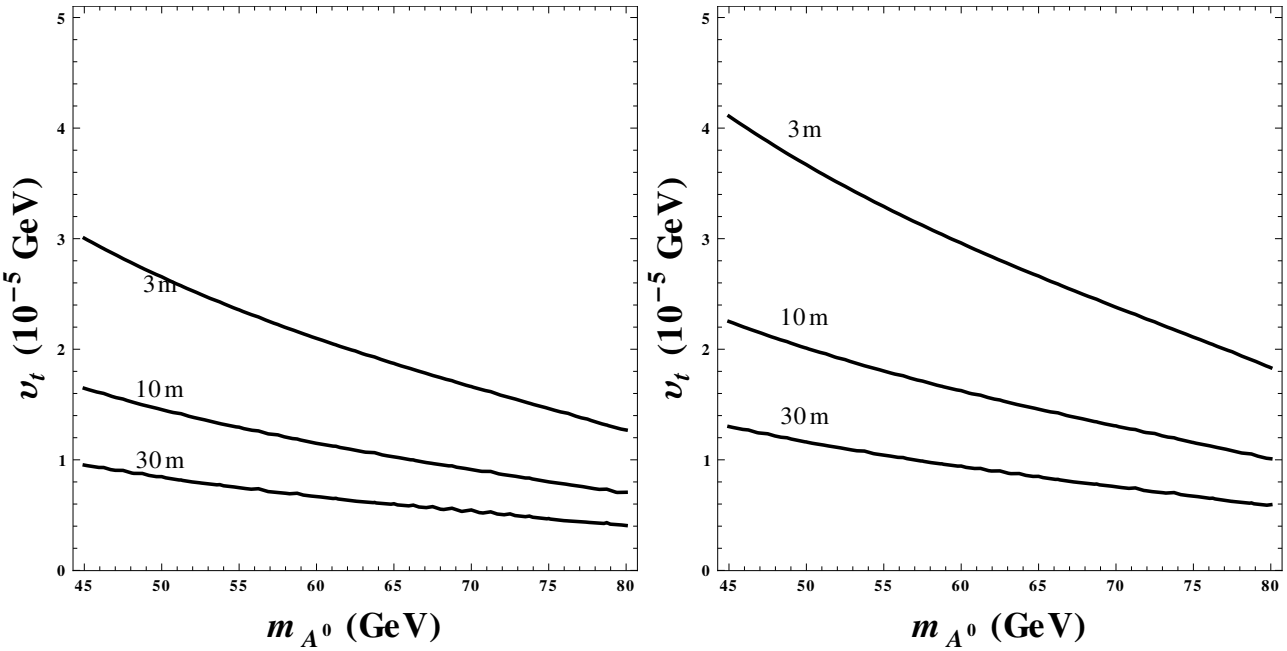

FIG. 8: A^0 decay length $c\tau$-contours in meters in the (m_{A^0}, v_t) plane: tree-level (left), including QCD corrections (right), assuming A^0 produced through $e^+e^- \to h^0 A^0$ at the LEP2 C.M. energy $\sqrt{s} = 183$GeV and a visible decay mainly into $b\bar{b}$.

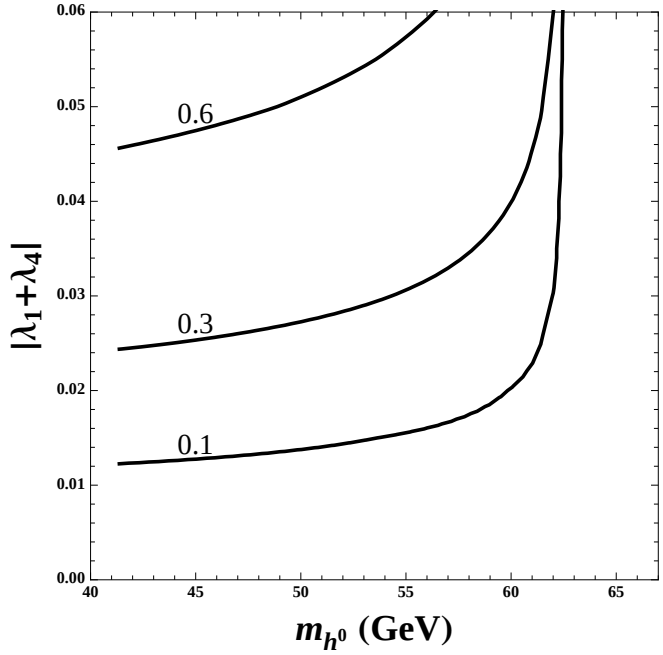

FIG. 9: Branching ratio contours for the invisible/undetected $\mathcal{H} \to h^0 h^0 + A^0 A^0$ decays in the m_{h^0} versus $|\lambda_1 + \lambda_4|$ plane, with $g_{\mathcal{H}hh} = g_{\mathcal{H}AA} = (\lambda_1 + \lambda_4) v_d$, $v_d = 246$ GeV, in the limit $\sin\alpha = 1$, $\sin\beta = 0$, taking $\Gamma_{\mathcal{H}}^{visible} = 4$ MeV and $m_{H^0} = 125$GeV.

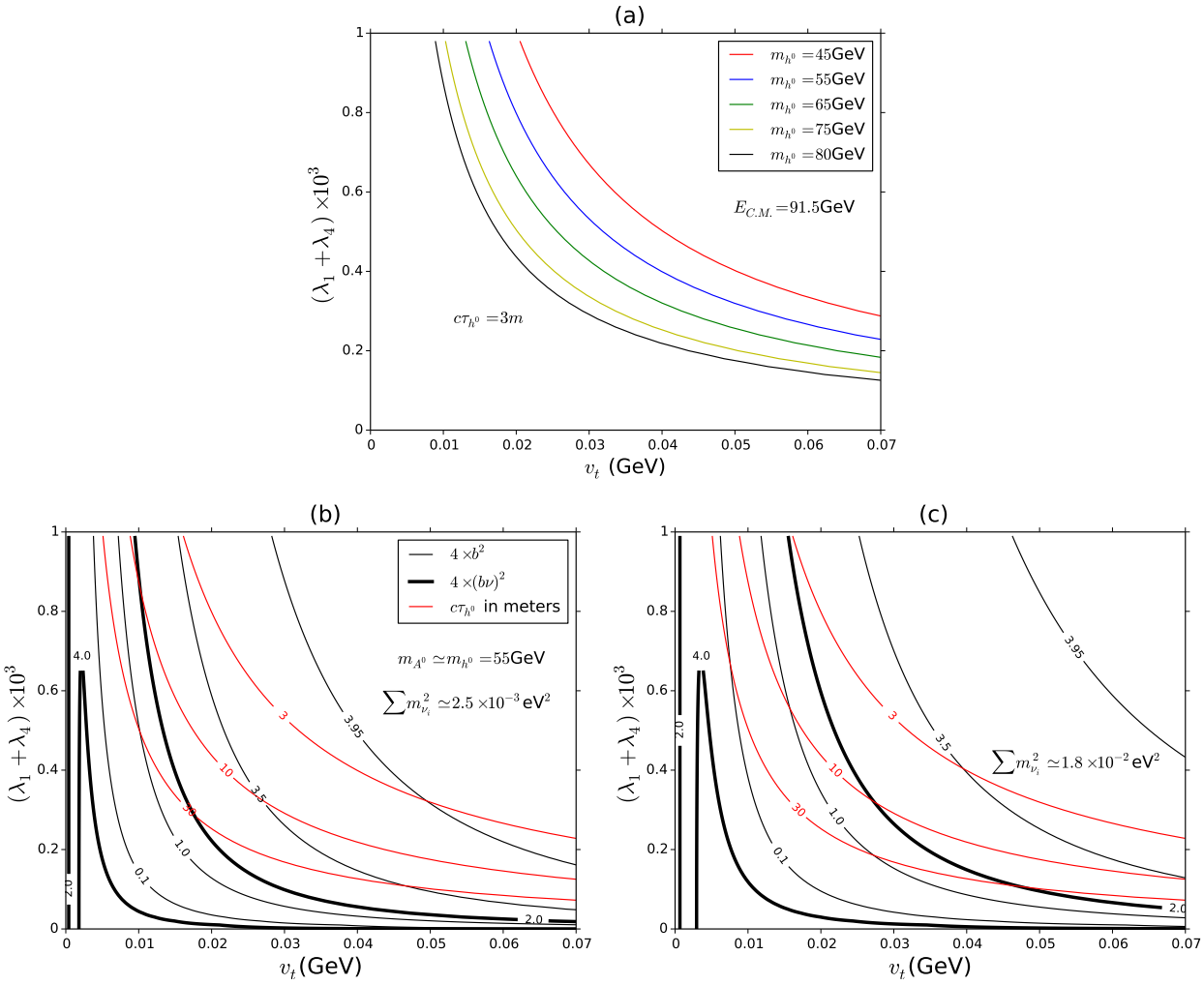

FIG. 10: (a) decay length contours in the $(v_t, \lambda_{14}^+ \times 10^3)$ plane, with a fiducial value $c\tau = 3$ meters for h^0 decaying visibly with energy $E_{C.M.} = 91.5$ GeV , shown for different h^0 masses; (b) contour plots for $4 \times Br(A^0 \to b\bar{b}) \times Br(h^0 \to b\bar{b}) = 0.1, 1, 3.5, 3.95$ (thin black lines), $4 \times Br(A^0 \to b\bar{b}) \times Br(h^0 \to \nu\nu + \bar{\nu}\bar{\nu}) = 2, 4$, (thick black lines), and h^0 decay length in meters, $c\tau = 3, 10, 30$m (red lines), in the $(v_t, \lambda_{14}^+ \times 10^3)$ plane, for $m_{A^0} \simeq m_{h^0} = 55$GeV and $\sum m^2_{\nu_i}|_{\rm min} \simeq 2.5 \times 10^{-3}$eV^2, in the limit of SM-like H^0. (c) same as (b) but with $\sum m^2_{\nu_i}|_{\rm max} \simeq 1.8 \times 10^{-2}$eV^2.

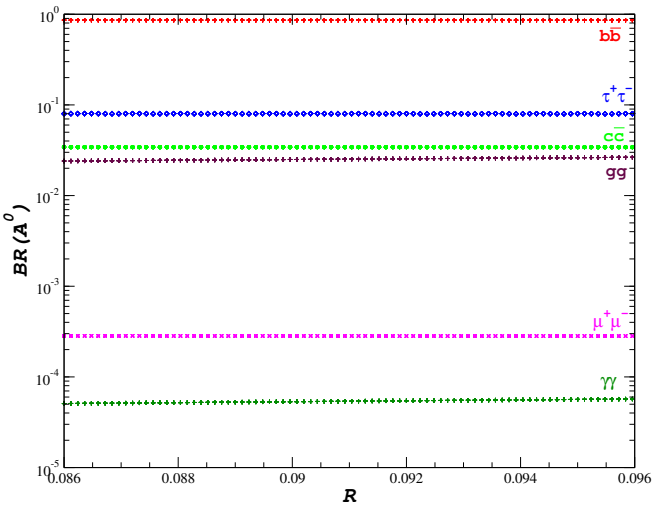

FIG. 11: The branching ratios $BR(A^0)$ as a function of the ratio $R \equiv \frac{\mu}{v_t}$ for fixed $m_{H^0} = 125.5$ GeV and various $\lambda_1 + \lambda_4$, with $\lambda_2 = 0.1$, $\lambda_3 = 2\lambda_2$, $-10 \leq \lambda_4 \leq 2$.

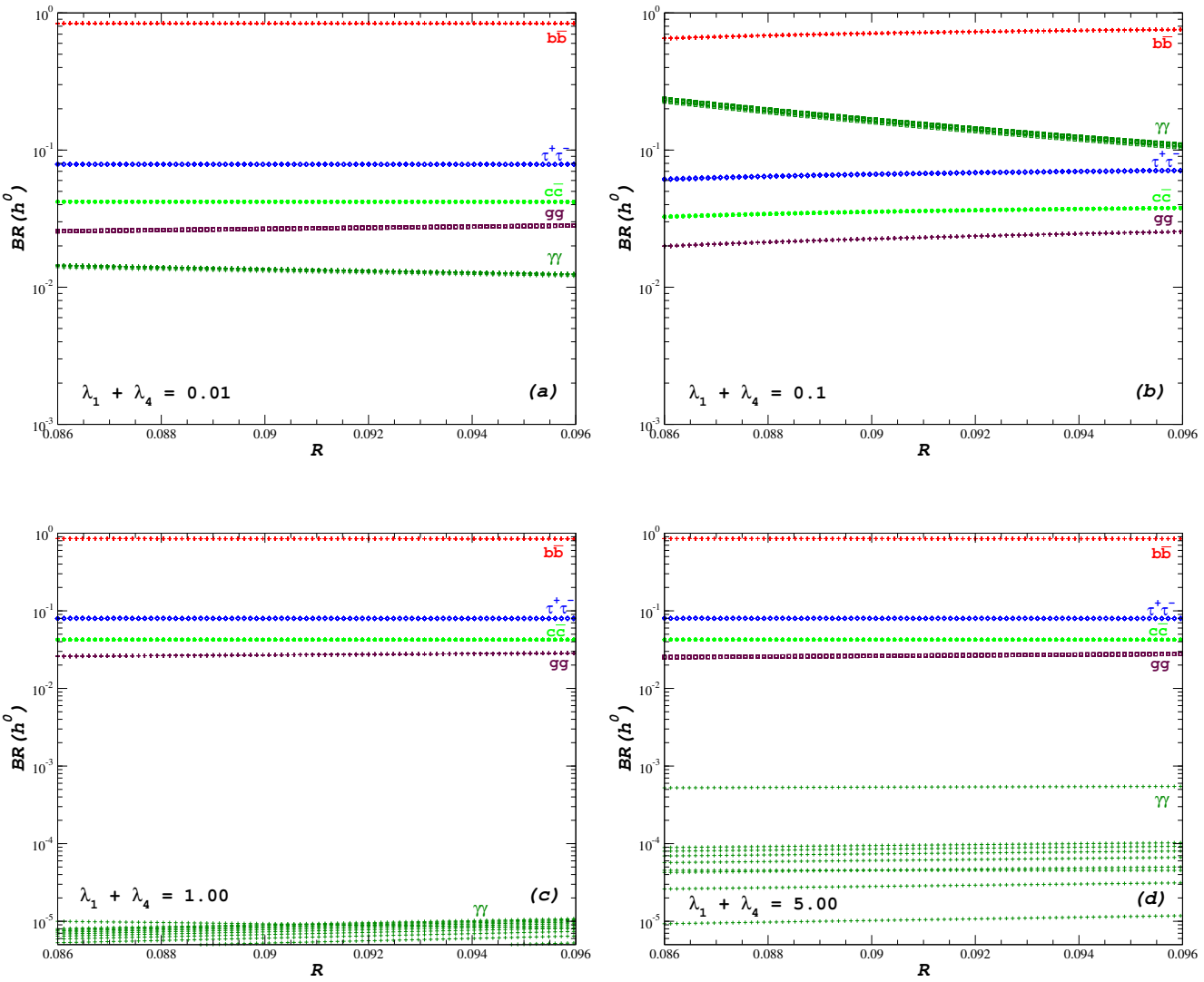

FIG. 12: The branching ratios $BR(h^0)$ as a function of the ratio $R \equiv \frac{\mu}{v_t}$ for fixed H^0 mass $m_{H^0} = 125.5$ GeV and various $\lambda_1 + \lambda_4$, $\lambda_2 = 0.1$, $\lambda_3 = 2\lambda_2$, $-10 \leq \lambda_4 \leq 2$.